CURTIN UNIVERSITY OF TECHNOLOGY

SCHOOL OF MATHEMATICS AND STATISTICS

DISCRETE DYNAMIC MODELLING OF GRANULAR FLOWS IN SILOS

Michael G Remias

A thesis submitted in fulfilment of the requirements for the award of the degree of

Master of Science (Mathematics)

of the

Curtin University of Technology

February 1998

ABSTRACT

This thesis develops and tests a two-dimensional discrete dynamic model for the simulation of granular flows in silos and hoppers. The granular material considered is assumed to be an assembly of viscoelastic discs and the motion of such a particle system is shown to be governed by a set of nonlinear first order ordinary differential equations. This system of equations is then solved numerically using the centered finite difference scheme. Based on the model presented, a computer program has been developed and used to analyse the flow behaviour of granular materials during filling and emptying of a silo. The results show that the discrete dynamic model developed is capable of modelling granular flows in silos, particularly predicting wall pressures and analysing flow blockage.

ACKNOWLEDGMENTS

I would like to thank my supervisor Dr Yong Hong Wu and Professor Brian White for their assistance, support, encouragement and patience during the course of my research and thesis preparation.

TABLE OF CONTENTS

LIST OF FIGURES

LIST OF TABLES

Chapter 1

INTRODUCTION

1.1 Background

Storage and flow of granular materials in silos are very important in many engineering applications. Problems which commonly occur in silo operation mainly include flow blockage, segregation, dead zones and silo collapse. These problems occur principally because our current understanding of granular flow is still not adequate.

Over the last few decades, a great deal of research has been carried out to investigate the properties of granular materials and their flows through silos. Early research has been mainly focused on experimental investigation and deriving approximate analytical methods for engineering design. A range of approximate methods have thus been developed, such as Janssen's differential slice force equilibrium method for wall pressures and Beverloo's equation for mass discharge rate. However, approximate methods in general cannot model the flow behaviour of granular materials. Hence in the last two decades, many researchers focused on

simulation of granular flows and as a result a number of mathematical models have been proposed. These models can be classified into two categories: the continuum models and the discrete element models. In continuum models, granular materials are assumed as continua either elastic-plastic solids or non-Newtonian fluids depending on the flow rate of the materials. Due to the complexity of granular flow, the flow theory of granular materials is still controversial and thus further work is still needed to investigate the flow behaviour of such a material.

1.2 Objectives and Scope

The main objective of this project is to develop a discrete dynamic model for simulating granular flows and to investigate the flow behaviour of materials in silos using the developed model. The project includes the following aspects of work:

- Develop a computer based numerical method for simulating the flow behaviour of particulate materials in silos.
- Investigate the flow patterns and velocity fields for different silo configurations.
- Investigate the effects of wall friction, material internal friction and silo geometry on wall pressure distributions.

1.3 Outline of the Thesis

This thesis consists of five chapters and is organised as follows:

Chapter one briefly introduces the background of research and defines the objectives and scope of the current work.

Chapter two presents a review of work on the modelling of granular flows and particularly flows through silos. More specifically, this chapter describes the general features of granular materials and the flow behaviour of materials in silos. Various methods for the study of flow behaviour are also described.

Chapter three describes the numerical algorithm developed in the present study for simulating granular flows through silos. Various aspects of the model are described in this chapter, including contact detection, contact force model, simulation of particle motion and calculation of wall pressures. The complete set of governing equations and the design of a simulation program are also presented in this chapter.

Chapter four investigates the flow behaviour and the wall pressure distributions during filling and discharging of a silo for different silo configurations and system parameters.

Chapter five provides a summary and conclusion of the study.

Chapter 2

PREVIOUS STUDIES ON GRANULAR FLOWS THROUGH SILOS

2.1 Granular Material and its Properties

A granular material is defined as an assembly of particles regardless of their shapes and size. Grains, sugar, cement and mineral products are all examples of granular material. This kind of material is very varied in their characteristics and to a certain extent their behaviour under flow conditions. Granular materials are neither solids nor liquids but share some aspects of both. Under certain conditions, granular materials flow like liquids and exhibit interfacial instability but, under other conditions they endure stress and support themselves with a finite angle of repose and behave like solids. The behaviour depends on the local stress condition, namely the yield condition. If the stress state is such that the yield condition is not satisfied, the material will essentially behave like a solid. On the other hand, if the yield condition is satisfied, the material will start to flow. At different stress states the material will behave according to different constitutive laws.

2.1.1 Yield functions

Granular materials fail due to frictional slip between particles. At yielding, the shear component of stress τ varies according to the value of the normal component of the stress σ. The locus of the value (σ,τ) at which permanent deformation or yielding occurs is called the yield locus and can be described by a function, namely yield function. In the space of principal stresses $(\sigma_1,\sigma_2,\sigma_3)$, a yield function is a surface. Various yield functions have been proposed to describe the yielding characteristics of granular materials. The most widely used yield function is the so called Mohr-Coulomb yield criterion which has the form of

$$\tau = c + \sigma \tan\phi \ , \tag{2.1}$$

where τ and σ are respectively the shear stress and normal stress, c represents the cohesion and ϕ is the angle of internal friction of the material. In the 3-D principal stress space, the Mohr-Coulomb yield function is an irregular hexagon as shown in figure 2.1.

Many other nonlinear models have also been developed in an attempt to describe the yield characteristics more accurately such as the Drucker-Prager (1952) and the Matsuoka-Nakai (1985) yield criteria. One of the most promising yield functions is the so called Warren-Spring yield function, developed by Hill and Wu (1993). This function takes the form of:

$$\left(\frac{\tau}{c}\right)^n = 1 - \frac{\sigma}{t} \ . \tag{2.2}$$

In terms of principal stresses, equation (2.2) becomes

$$F(\sigma_I,\sigma_{III}) = x^{n/(2-n)} + (\lambda^2/n)x - B \ , \tag{2.3}$$

where $\lambda = c/t$ and x is defined by

$$x = \frac{B - [B^2 - 4(l/n)^2(n-1)A]^{1/2}}{2(l/n)^2(n-1)} \quad , \tag{2.4}$$

in which A and B are given in terms of σ_I and σ_{III} by

$$A = \left(\frac{\sigma_I - \sigma_{III}}{2\lambda t}\right)^2 \quad , \quad B = 1 - \frac{\sigma_I + \sigma_{III}}{2t} \quad . \tag{2.5}$$

In the principal stress space, the Warren-Spring yield function is as shown in figure 2.2. It is obvious that the yield function (2.2) reduces to the Mohr-Coulomb yield function if n=1.

2.1.2 Macro-behaviour and micro-mechanics characteristics

At different stress states, the macro-behaviour of a granular material is very different. If the stress level is below the yielding limit, the material behaves like an elastic body. While, when the stress level exceeds the yielding limit, it behaves usually like a viscoplastic fluid. Figure 2.3 shows the typical relationship between stress and deformation.

To describe the macro-mechanic property of granular material mathematically, we first need to establish a yield function distinguishing the elastic region from the viscoplastic region and then develop proper equations, namely the constitutive equations, to describe the stress-deformation relations for each of the regions. Over the last few decades, a great deal of work has been carried out to develop proper constitutive equations, such as the hyper-elastic model for the elastic

region, the plastic flow rule theory and the double shearing theory for the viscoplastic region.

There are numerous types of granular materials. They are often formed by processes of crushing or mining operations. The macro-mechanics property of such a material depends on the micro-mechanics properties including particle size, size distribution, particle shape, particle surface structure and particle deformation characteristics. So various attempts have been made to study the influence of micro-mechanics characteristics on macro-behaviour. Research in this area can be classified into two types, experimental investigation and micro-mechanics based investigation. Due to the complexity, most micro-mechanics characteristics such as particle shape still cannot be included in macro-mechanics models. However, in principle, the discrete dynamic model can be used to consider the influence of micro-mechanics property on macro-behaviour.

When subjected to external loads, a granular material will undergo deformation. Once the particle-particle and particle-boundary bonds are overcome, flow occurs. Tlus, the material first shears like a solid, then it behaves as a liquid or a plastic material. The initial failure of the material may result in particle 'blocks' (i.e, a number of particles) moving relative to others. If the flow is rapid enough, this may lead to a complete breakdown of 'bonds' and result in each particle moving freely and independently of its neighbours. In rapid flows, the main transport mechanism is particle collisional interactions, whereas in slow flows the main mechanism is close contact between particles.

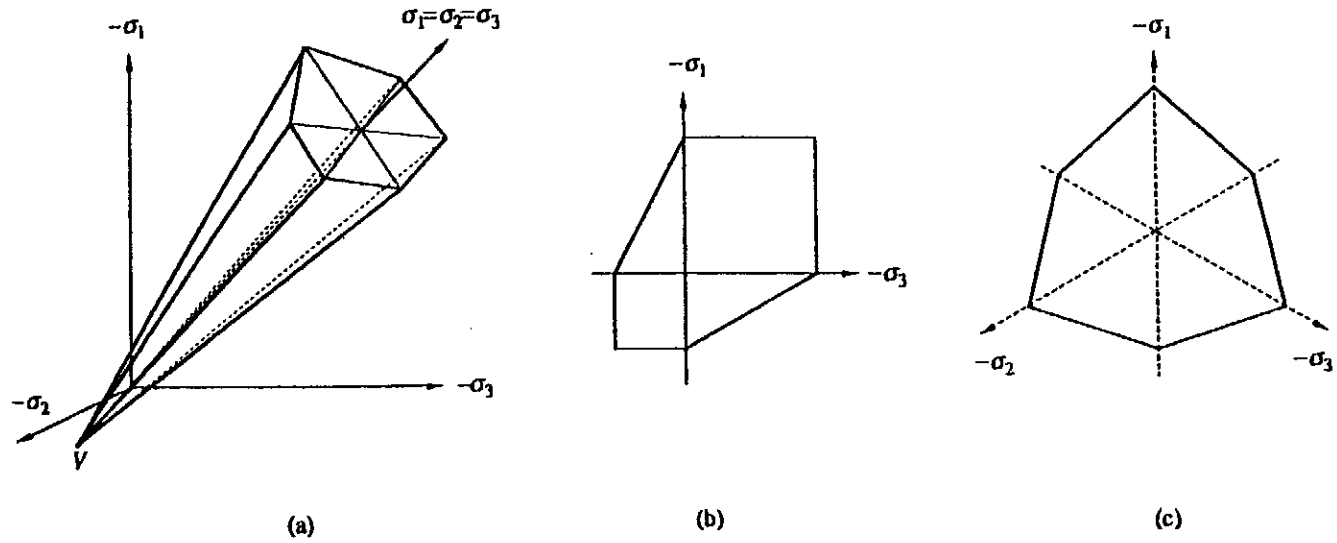

Figure 2.1 : Coulomb–Mohr yield surface (a) in principal stress space, (b) intersection by $\sigma_2 = 0$, (c) intersection by plane $\sigma_1+\sigma_2+\sigma_3 = 0$.

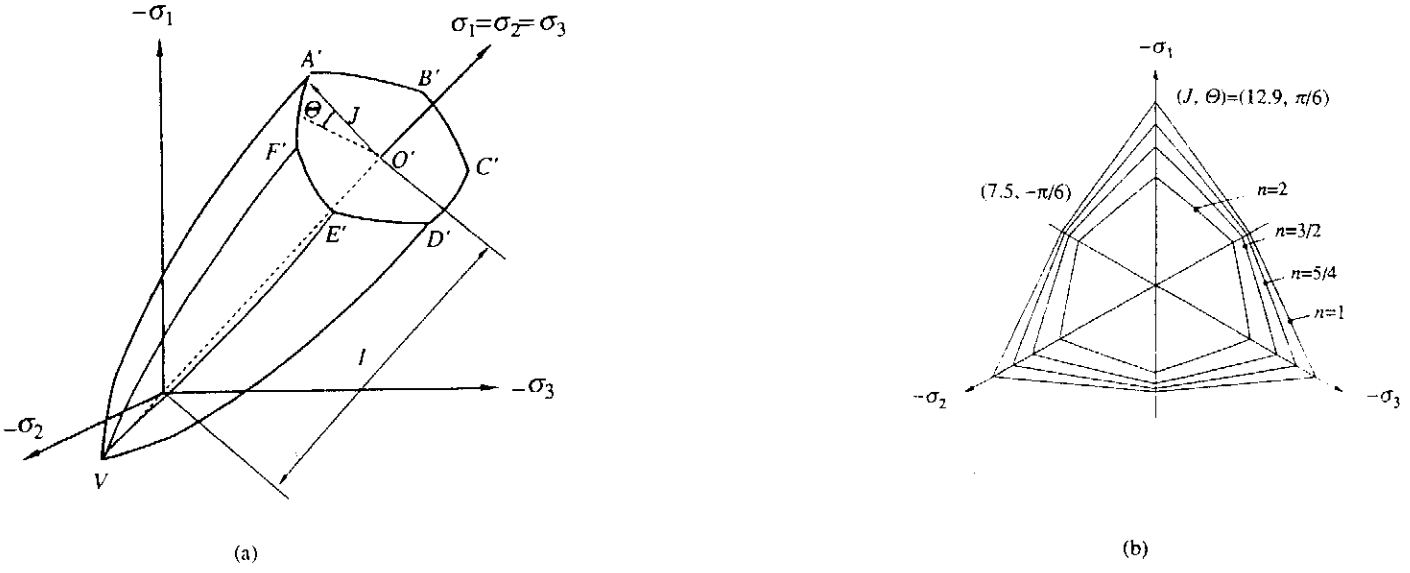

Figure 2.2 : Warren-Spring yield surface (a) in principal stress space (b) intersection by $I = \sigma_I + \sigma_{III} = -10$

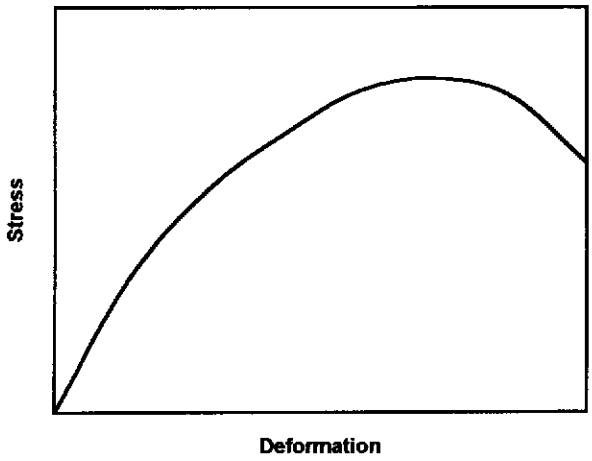

Figure 2.3 : Stress vs Deformation

2.2 Flow Modes and Wall Pressures in Silo Operation

As shown in figure 2.4, there are two types of flows identified in silos, namely, mass flow and funnel flow. In mass flow, the movement of the granular material in silos is fairly uniform whereas in funnel flow, there is a central flowing region surrounded by a relatively stable region. The mode of flow in a silo depends on various factors such as silo geometry, material characteristics and boundary contact conditions.

Depending on the abrasive nature of the silo contents it may be desirable to have a wall protecting funnel flow. However, in some other cases, for example, if a silo is used for storing foods, then it is desirable to have mass flow. Therefore, it is extremely important to be able to simulate the material flow pattern for different operation conditions and system parameters.

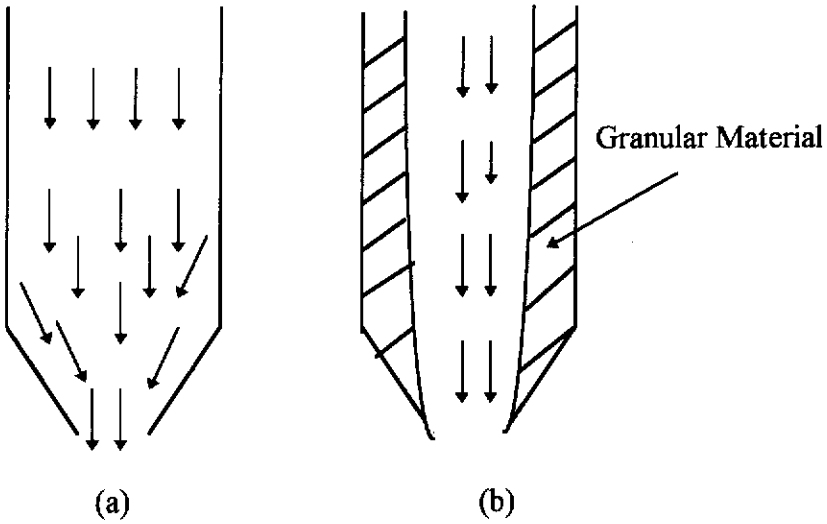

Figure 2.4. Flow Modes in Silos (a) mass flow (b) funnel flow

2.3 Pressure Distributions on Silo Walls

Prediction of wall pressure distributions is essential for the design of silos and hoppers. Over the last few decades, extensive research has been carried out to study the distribution of pressures on silo walls during filling and emptying of a silo.

Early research is mainly experimental. However in the last two decades, many numerical investigations based on the continuum mechanics approach have been conducted. Figure 2.5 shows the general features of pressure distribution on silo walls obtained by using the continuum mechanics approach (Schmidt and Wu, 1989). It can be noted that there are three different stages of pressure response to the material discharge. In the first stage, the pressure near the outlet increases more quickly than that in the transition area. In the second stage, pressure in the

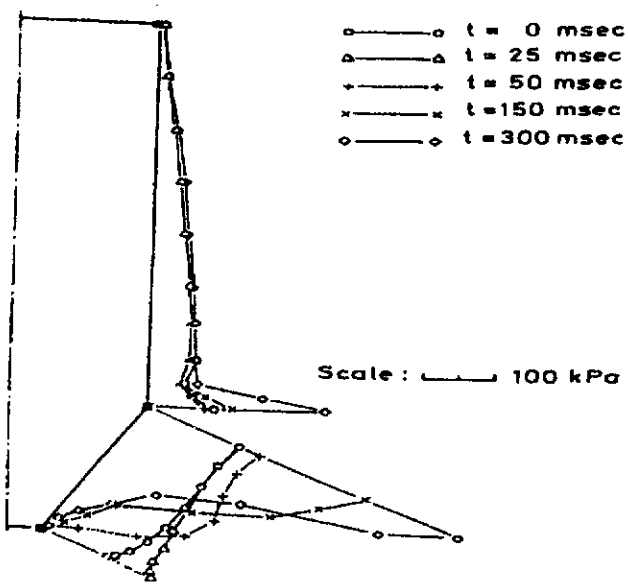

Figure 2.5 : General features of pressure distributions on silo walls

transition area is nearly constant. But, the position of the peak pressure on the hopper wall moves slowly from the outlet to the transition point, and the pressure near the outlet decreases. During the third stage, there is a strong increase of wall pressure at the transition and a decrease near the outlet.

2.4 Methods for the Study of Granular Flows

The flow problems of granular materials have been modelled with a number of methods. Early research is mainly focused on deriving empirical formulas for engineering design and is based on the so called approximate analytical method. With the development of computer technology and numerical methods, more and

more attempts have been made to study granular flows using the continuum mechanics method and the discrete element method.

2.4.1 Approximate Analytical Methods

Various researchers have developed approximate analytical formulas for the determination of pressures on silo walls, including those by Janssen (1895), Walker (1966), Walker and Blanchard (1967), Jenike (1964, 1969) and others.

In 1895, Janssen derived a formula for the predictions of silo pressures based on three major assumptions

(1) the distribution of vertical stress across any cross-section is uniform;

(2) the ratio of horizontal stress to vertical stress is constant throughout a silo;

(3) material is homogeneous and isotropic and can be treated as a continuum.

Walker (1966) and Walker and Blanchard (1967) assumed a flow pattern in which all solids in a bin is in motion whenever discharge conditions exist and then derived a formula for silo flow pressures. His work agrees reasonably well with experimental observations. Jenike and Johanson (1969) have developed predictive methods for both static and dynamic pressures on silo walls. Jenike's formula predicts that the flow pressure on the wall of a bin-hopper combination consists of a pressure maximum at the transition of the vertical bin wall and the hopper wall

followed by a linear decrease to an intermediate value and another linear decrease to zero at the apex. Jenike's formula was developed based on the assumption that the overpressure at the transition is distributed over 0.3 D (diameter of the silo) of the hopper wall from the transition point.

2.4.2 Continuum Mechanics Methods

In continuum mechanics models, a granular material is identified as a continuum and the particulate nature of the flowing bulk is ignored completely. The material micro-mechanics characteristics are taken into account indirectly via the parameters used in the constitutive equations for the model. At present, there are two important types of constitutive models for granular flows, namely

(a) collisional models based on the kinetic theory of dense gases,

(b) frictional models based on plasticity theory.

The collisional model is developed for rapid flows and have been explored largely since late 1970s. Constitutive equations based on this kind of model are capable of predicting the features of certain simple flows such as plane shear flows. However the results are generally only valid for simple rapid flows. The frictional model is mainly for slow granular flow and is based on the plasticity theory. However, it has been generally realised that under certain conditions the frictional continuum approach may not be able to yield accurate predictions on granular flows in silos. This is due to the assumption of uniform failure properties and the use of quasi-static flow rules in calculations.

2.4.3 Discrete Elemental Methods

The discrete element method grew out of work on molecular dynamics with one of the first applications to a macroscopic system being carried out by Cundall and Strack (1979). The discrete element method aims to follow the motion of every particle in the system and by applying force displacement laws, determines the new particle positions at a time, δt, later. This has become more practical with the creation of high speed and parallel computer systems. Potentially the concept of following individual particles within a system could more extensively describe the overall motion and characteristics of the granular assembly. However there is a price to pay in terms of the computational power required.

The discrete element method tracks the motion and interactions of every single particle in its system. Contacts with neighbouring particles is determined at each time step and by using force-displacement laws the resultant velocity of the particle is calculated. The particle motions are determined over a very small time interval. The determination of an appropriate time interval is important since if the interval is not sufficiently small, the system will not tend towards equilibrium. Because of the use of discrete particles within the system, the discrete element method is useful in describing flow behaviour under a broad range of conditions. The following are some typical areas of application (Rong, 1994),

- behaviour of soils, rocks and granular materials
- impact and explosive dynamics

- earthquake and geotechnical engineering
- granular flow and river ice transport

The discrete element method has the advantage over experimental methods in that the data is collected un-obtrusively and there is no need for the design of complex testing equipment. In addition, the method is able to obtain data from all areas of the flow and at any instant of time. The collected information may be averaged or otherwise used as a time series to describe the overall system characteristics. Another advantage is that the discrete element method does not require a constitutive equation for the whole computational domain, unlike other numerical techniques.

A disadvantage of the discrete element method is that it requires significant computational power even for a very small assembly. Thousands of calculations are required every time step in order to determine the contacts and motion of each particle within the flow region, and there will be thousands of time steps required to simulate even a few seconds of actual flow. The method is therefore more suited in modelling dynamic behaviour rather than static or long term characteristics. By the nature of repetitive calculations on each particle, this method seems to be well suited for analysis by parallel computer systems. So far, most models do not consider variation of individual particle shapes, although in many types of flows such as slippage of snow and ice flows particle shape may restrict or encourage particulate flow characteristics. Hogue and Newland (1994)

have investigated a range of particles shapes, such as spherical, cylindrical and regular polygonal but were not able to combine these shapes in the simulation.

Discrete element models can be classified into two categories, namely, the soft particle models and the hard particle models.

2.4.3.1 Soft Particle Models

In soft particle models, particles are assumed to experience collisions of finite duration with elastic deformation. The deformation is represented as an overlap of the particulate edges. At each time step, forces acting on each particle by particle-particle contact, particle-wall impact and gravitation are numerically integrated to obtain the velocity of each particle. The particle motion is governed by Newton's equation of motion and a force-displacement law. The key problem in the soft particle approach is the modelling of particle-particle interaction and the particle-wall interaction. Several contact force models have been proposed including the elastic model and the Hertzian model.

Cundall and Strack (1979) modelled a granular material as an assembly of particles, connected by springs and dashpots. The spring and dashpots are used to create the desired force versus displacement characteristics. The internal forces developed between particle pairs or between particle and wall in contact are calculated based on the force-displacement law.

The normal spring stiffness is approximated with the maximum normal contact force F_n expected, and the maximum allowable overlap between particles δ_n, expressed as

$$K_n = \frac{F_n}{\delta_n} \quad . \tag{2.6}$$

Corkum and Ting (1986) suggested that the maximum overlap should be between 2 % and 5 % of the disk radius. Johnson (1985) recommended that the value of tangential stiffness lies between $2/3K_n$ and K_n depending on the Poisson's ratio. The relationship above provides a simple approximation of the contact stiffness. Various other forms of formulas have been developed for the calculation of spring stiffness.

Babic (1990) calculated the normal and tangential contact stiffness K_n and K_s from particle stiffness k_n and k_s using the analogy with springs connected in series. The contact stiffnesses for identical particles are $K_n = ½k_n$ and $K_s = ½k_s$. It should be noted that the linear contact law is not inherent in the model. A non-linear law such as the Hertzian contact law could be employed equally well. However, the linear contact law has been widely used in discrete element method, since it is simple and can be easyly incorporated in computer code and allows for rapid computation. Tsuji, Tanaka and Ishida (1992) proposed an estimation of stiffness using Hertzian's contact theory when the physical properties such as Young's modulus and Poisson ratio of the particle are known. The normal and tangential stiffness between two spheres are

$$K_n = \frac{\sqrt{2r}E_s}{3(1-\sigma_s^2)}, \quad K_s = \frac{2\sqrt{2r}G_s\delta_n^{1/2}}{2-\sigma_s}, \tag{2.7}$$

where E_s and σ_s are the Young's modulus and Poisson ratio of the particles respectively, r is the particle radius, G_s is the shear modulus and δ_n denotes normal displacement. The normal and tangential stiffness between a sphere and a wall are given by

$$K_n = \frac{\frac{4\sqrt{r}}{3}}{\frac{1-\sigma_s^2}{E_s}+\frac{1-\sigma_w^2}{E_w}}, \quad K_s = \frac{8\sqrt{r}G_s\delta_n^{1/2}}{2-\sigma_s}, \tag{2.8}$$

where E_w and σ_w are respectively the Young modulus and the Poisson ratio of the wall.

Various methods have been proposed to calculate the normal force acting on a particle. The following lists some commonly used models.

(1) Hooke's spring interaction law

$$F_n = k(\sigma - r), \tag{2.9}$$

where k is the bulk stiffness, F is the particle diameter and r is the center distance between two particles.

(2) Partially latching spring model (Walton and Braun, 1986).

In this model, different stiffnesses are used for the loading and unloading portion of an impact, namely,

$$F_n = \begin{cases} K_1\delta & \text{for loading} \\ K_2(\delta - \delta_o) & \text{for unloading} \end{cases} , \tag{2.10}$$

where δ is the relative overlap after initial contact and δ_o is the value of δ when the unloading curve goes to zero.

(3) The Hertzian interaction force model (Langston, Tuzun and Heyes, 1995),

$$F_n = \frac{4}{3} E \sqrt{R(\sigma - r)^{3/2}} , \tag{2.11}$$

where E is the elastic modulus, R is the contact radius of curvature, σ is the particle diameter, and r is the centre distance between two particles.

(4) The Continuous normal interaction model (Langston, Tuzun and Heyes, 1995)

$$F_n = \frac{n\varepsilon \left(\frac{\sigma}{r}\right)^n}{r} , \tag{2.12}$$

where n is an arbitrary index, and $\varepsilon = \frac{\sigma mg}{n}$.

The tangential force is modelled using Amonton's law proposed by Mindlin and Deresiewicz (1953) as

$$F_s = \mu F_n \left(1 - \left\{ 1 - \left| \frac{\delta_s}{\delta_{\max}} \right| \right\}^{3/2} \right) , \tag{2.13}$$

where $\delta_{max} = C_s \mu F_n$, δ_s is the total tangential displacement, and C_s is the average tangential compliance given by $\frac{\delta_{max}}{F_s}$.

2.4.3.2 Hard Particle Models

In these kind of models (Campbell and Gong, 1986; Hopkins and Shen, 1986; Hopkins and Louge, 1991), collisions are assumed to be instantaneous and there is no interpenetration of particles. Particle paths following contact are calculated based on their initial path and the resultant collision dynamics. Energy can be lost through a coefficient of restitution. Rapid flows of granular materials can result in high deformation rates. This causes particle-particle and particle-wall collisions and generate random motion. This random motion generates the so called granular temperature and is the measure of the fluctuation energy in the material (Ahn, Brennen and Sabersky, 1992). The hard particle models are particularly suited to systems with high granular temperature and low density.

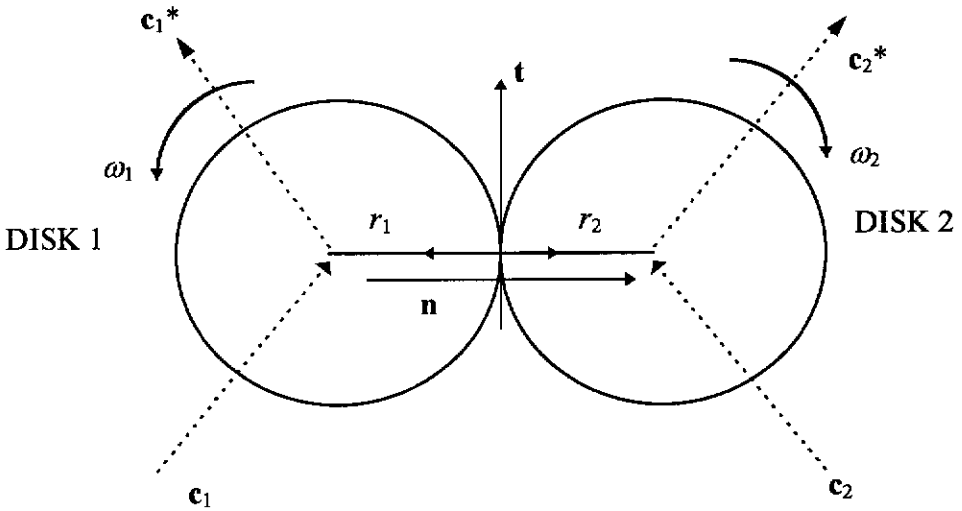

Figure 2.6 Hard Particle Interaction

When two particles collide as shown in figure 2.6, the principle of linear momentum must be satisfied and thus

$$m_1\mathbf{c}_1^* + m_2\mathbf{c}_2^* = m_1\mathbf{c}_1 + m_2\mathbf{c}_2 \quad , \qquad (2.14)$$

where $\mathbf{c}_i$ and $\mathbf{c}_i^*$ denote respectively quantities before and after impact. Conservation of angular momentum about the contact point yields

$$m_1\mathbf{r}_1 \times \mathbf{c}_1^* + I_1\omega_1^* = m_1\mathbf{r}_1 \times \mathbf{c}_1 + I_1\omega_1 \quad , \qquad (2.15)$$

$$m_2\mathbf{r}_2 \times \mathbf{c}_2^* + I_2\omega_2^* = m_2\mathbf{r}_2 \times \mathbf{c}_2 + I_2\omega_2 \quad . \qquad (2.16)$$

To describe inelastic collisions, a coefficient of restitution ε is usually introduced, with an equation that expresses the incomplete restitution of translational velocities in the normal direction

$$(\mathbf{c}_1^* - \mathbf{c}_2^*).\mathbf{n} = -\varepsilon(\mathbf{c}_1 - \mathbf{c}_2).\mathbf{n} \quad . \qquad (2.17)$$

The collisional impulse, $\mathbf{P}_i$, on the ith particle is given by

$$\mathbf{P}_i = m_i(\mathbf{c}_i^* - \mathbf{c}_i) \quad . \qquad (2.18)$$

The sliding friction between particles is described by

$$\mathbf{P}_t = \mu\mathbf{P}.\mathbf{n} \qquad \text{(the SLIP case)} \qquad (2.19)$$

where $\mathbf{P} = \mathbf{P}_1 = m_1(\mathbf{c}_1^* - \mathbf{c}_2) = m_2(\mathbf{c}_2 - \mathbf{c}_2^*) = -\mathbf{P}_2$. The NOSLIP case is given by

$$\mathbf{c}_{12c} = \mathbf{c}_1 + \mathbf{r}_1 \times \omega_1 - \mathbf{c}_2 - \mathbf{r}_2 \times \omega_2 \qquad (2.20)$$

where $\mathbf{c}_{12c}$ is the relative velocity between the particles at the contact point.

To determine if the situation is SLIP or NOSLIP, one uses

$$\mathbf{P}_t\,[\text{NOSLIP}] > \mathbf{P}_t\,[\text{SLIP}] \quad \Rightarrow \quad \mathbf{P}_t = \mathbf{P}_t\,[\text{SLIP}]$$

$$\mathbf{P}_t\,[\text{NOSLIP}] \leq \mathbf{P}_t\,[\text{SLIP}] \quad \Rightarrow \quad \mathbf{P}_t = \mathbf{P}_t\,[\text{NOSLIP}]$$

2.5 Time Step

As mentioned earlier, the time step chosen in the discrete element method is important to optimise the simulation. If the steps are too large the material flow characteristics may not be accurately modelled. For example, particles may, between time steps, appear to travel through the walls of the silos or possibly bypass a particle-particle interaction. On the other hand, if the time step chosen is too small the simulation can become very slow, requiring greater computational power. Cundall and Strack (1979) proposed the following method to calculate the critical time step, t_c

$$t_c = \sqrt{\frac{m_{\min}}{K_{\max}}} \quad , \tag{2.21}$$

where $m_{\min}$ is the lightest mass of a particle in the system, $K_{\max}$ is the largest spring stiffness (normal or tangential).

Babic (1990) suggested another formula for the calculation of the time step, namely

$$t_c = \frac{\pi}{\sqrt{\frac{K_n}{m}\left(1 - \frac{\ln^2 \varepsilon}{1 + \ln^2 \varepsilon}\right)}} \quad , \tag{2.22}$$

where K_n is the normal stiffness, m is the particle mass and) is the coefficient of restitution.

2.6 Summary

By examining the macro-characteristics of granular materials, the behaviour of granular flows in silos and the method of study, the following conclusions can be made

(1) Granular materials are neither solids nor liquids but share some aspects of both. A granular material can behave like a solid in some cases while like a liquid in other cases depending on the stress state.

(2) The modelling of granular flows in silos is important. However the flow behaviour of granular materials in silos is very complicated and requires further investigation using new techniques.

(3) Various methods can be used to study the flow of granular materials. However, approximate analytical methods cannot simulate the flow behaviour. Continuum mechanics methods require a set of global constitutive equations which are difficult to establish and not capable of directly modelling the influence of the material micro-mechanics characteristics on flow behaviour. While the discrete dynamic model can model the influence of material micro-characteristics on macro-behaviour, at least in principle.

(4) For slow flows of granular materials with high bulk density, the appropriate discrete dynamic model is the so called soft particle model.

Therefore the purpose of this study is to develop and test a soft particle discrete dynamic model for simulating granular flows in silos.

Chapter 3

DEVELOPMENT OF A DISCRETE ELEMENT MODEL

3.1 General

The main features of the discrete element model were developed by Cundall and Strack (1979). In the discrete element model a granular material is considered to be made up of many discrete particles that interact as they flow from a silo. The equations governing the motion of each individual particle are the principles of linear momentum and angular momentum. At a particular instance of time, the total forces acting on each particle are determined by considering the particle-particle and the particle-wall interactions. By integrating the differential equation for the motion of the particle, the new particle velocities and positions are obtained and the calculation process continued at the next time step.

In this chapter, we develop a discrete element model for simulating granular flows in silos. The model keeps track of the location and contacts of each particle and recalculates this information at each new time step. We will describe how to detect contacts, how to calculate contact forces and simulate particle motion. In

addition, methods for the calculation of wall pressures and stresses will be developed. The design of a computer program and its validation will also be given in this chapter.

3.2 Contact Detection

In the discrete element method, it is necessary to determine interaction of each individual particle with other particles and the system boundary such as silo walls, so that interaction forces acting on a particle by other particles can be determined. For the success of a discrete dynamic model, it is essential to develop an efficient algorithm for the detection of particle-particle and particle-wall contacts. In this section, we present a contact searching algorithm and its implementation in computers.

3.2.1 Particle-particle contact

The search for contacts of a particle i with other particles is performed by detecting the distance between the centre of particle i and its neighbouring particles. Thus, particles i and j are in contact if

$$s = \sqrt{(x_i - x_j)^2 + (y_i - y_j)^2} \le R_i + R_j \quad , \qquad (3.1)$$

where R_i and R_j are the radii of particles i and j, and (x_i, y_i) and (x_j, y_j) are the coordinates of their centres (see figure 3.1).

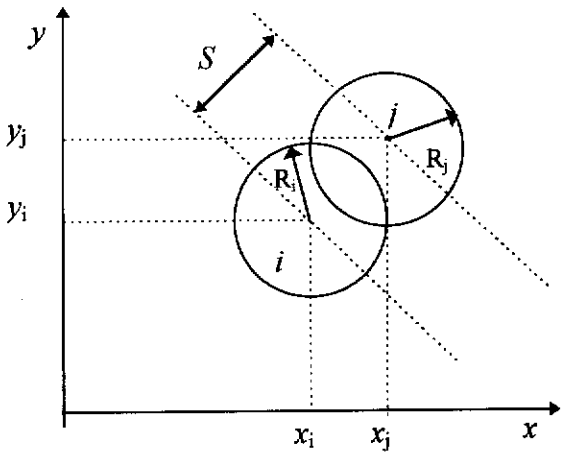

Figure 3.1 Particle-particle contact

The process of searching for contacts between particles is the most time consuming part of the simulation. The search strategy used in the present study is of the detector type, that is, a contact is registered whenever an overlap between two particles is detected.

The simplest and conventional method is to check for an overlap between all pairs of particles. This process requires $N_p(N_p\text{-}1)/2$ tests where N_p is the total number of particles in the system under consideration. For systems with a large number of particles, this method is obviously unacceptable since it is too time consuming. Therefore an efficient searching method is desired based on the idea of neighbourhood search, such as the linked listed method proposed by Allen and Tildesley (1988) for molecular dynamics and the grid algorithm by Hopkins (1987). The contact detection algorithm developed in the present study is based on the grid algorithm which is described as follows.

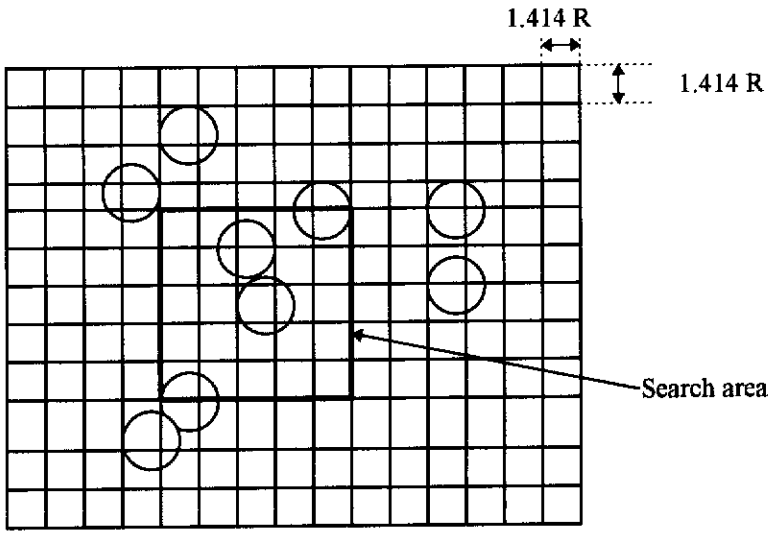

Figure 3.2 Contact search area

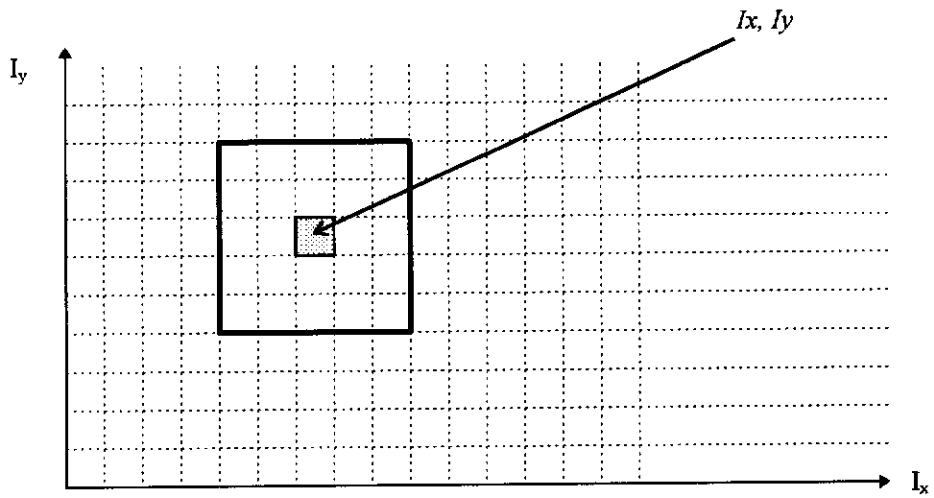

Figure 3.3 Grid Reference

To define a neighbourhood about a particle, a rectangular grid is superimposed onto a space occupied by particles. The size of the grid cell, $Gl \times Gl$, is chosen such that only one particle centre may occupy a cell at any given time and for this purpose, we require $Gl < 1.414\ R$ where R is the radius of the particle. Suppose

that *Gl* is equal to the radius of the particle, then the area that needs to be searched for contacts of a given particle consists of $5^2 - 1 = 24$ cells surrounding the cell occupied by the particle as shown in figure 3.2.

The grid is superimposed onto the computation region of dimensions (*Xlength*, *Ylength*) with the origin of the grid coordinate system started at the left bottom corner. The location of each cell is identified by two cell indexes *Ix* and *Iy* as shown in figure 3.3. The range of *Ix* and *Iy* are respectively

$$Ix\text{: } 1 \text{ to } Ixmax, \text{ where } Ixmax = \text{int}(Xlength/Gl) + 1 \quad ,$$

$$Iy\text{: } 1 \text{ to } Iymax \text{ , where } Iymax = \text{int}(Ylength/Gl) + 1 \quad .$$

The particle *i*, located at (*X(i), Y(i)*) can thus be identified by the cell index coordinate (*Ix, Iy*) where $Ix = \text{int}(X(i)/Gl) + 1$, $Iy = \text{int}(Y(i)/Gl) + 1$. This information is then stored into a 2D array by letting PDist (*Ix, Iy*) = *i*. Looping through all particles, we will generate the 2D array PDist(*Ix, Iy*) (*Ix*: 1 to *Ixmax*, *Iy*: 1 to *Iymax*) containing the information of distribution of all particles. For example PDist(*Ix, Iy*)= *I* means that the cell with grid coordinates (*Ix, Iy*) contains particle *I*, while PDist(*Ix, Iy*) = 0 means that the cell (*Ix, Iy*) does not contain any particles. With PDist, it is a simple matter to search for contact between particles. For example, consider particle *p* with grid coordinate *Ix, Iy*. The particles which may be in contact with *p* are only those contained in the neighbourhood of (*Ix, Iy*), that is those in the cells {(*i, j*)} $i = Ix-2$ to $Ix+2$, $j = Iy-2$, $Iy+2$. The following algorithm can thus be used to detect the particles in contact with *p*

(1) Find the grid location of p,

$$Ix = \text{int}(X(i)/Gl) + 1 , \tag{3.2}$$

$$Iy = \text{int}(Y(i)/Gl) + 1 . \tag{3.3}$$

(2) Search over the neighbourhood of (Ix, Iy)

do for i=Ix-2 to Ix+2

do for j=Iy-2 to Iy+2

(3) Identify the particles contained in (i,j)

p_{ij}=PDist(i,j)

(4) Test contact condition

calculate distance s between particle p and p_{ij} and then

compare s with ($Rp + Rp_{ij}$)

(5) If p_{ij} is in contact with p (s<$Rp + Rp_{ij}$), add it to the contact list of p,

namely let

numct(p): = numct(p) + 1

listct(p, numct(p)) = p_{ij}

3.2.2 Particle-wall contact

The contact between particle i and a straight wall w is shown in figure 3.4. The wall w is defined by its coordinates at the end points. The length of the wall, lw, and the angle θ_w with respect to the x-axis are respectively

$$l_w = ((x_2-x_1)^2 + (y_2-y_1)^2)^{1/2} \quad , \tag{3.4}$$

$$\theta_w = \tan^{-1} \frac{y_2 - y_1}{x_2 - x_1} \quad . \tag{3.5}$$

Let the distance between the particle centre and one of the wall end points in directions parallel and perpendicular to the wall be respectively S_t and S_v. Then from figure 3.4, S_t and S_v can be determined by

$$S_t = (x_p-x_1) \cos \theta_w + (y_p-y_1) \sin\theta_w \quad , \tag{3.6}$$

$$S_v = -(x_p-x_1) \sin \theta_w + (y_p-y_1) \cos \theta_w \quad . \tag{3.7}$$

The particle is in contact with the wall if

$$0 \le S_t \le l_w \quad \text{and} \quad 0 \le S_v \le R \quad .$$

3.3 Contact Force Model

Considering the particle to particle interaction, the interaction force acting on particle i by particle j can be decomposed into a normal and a shear component, namely

$$\mathbf{F}_{i,j} = F_{ijn}\mathbf{n} + F_{ijs}\mathbf{s} \quad , \tag{3.8}$$

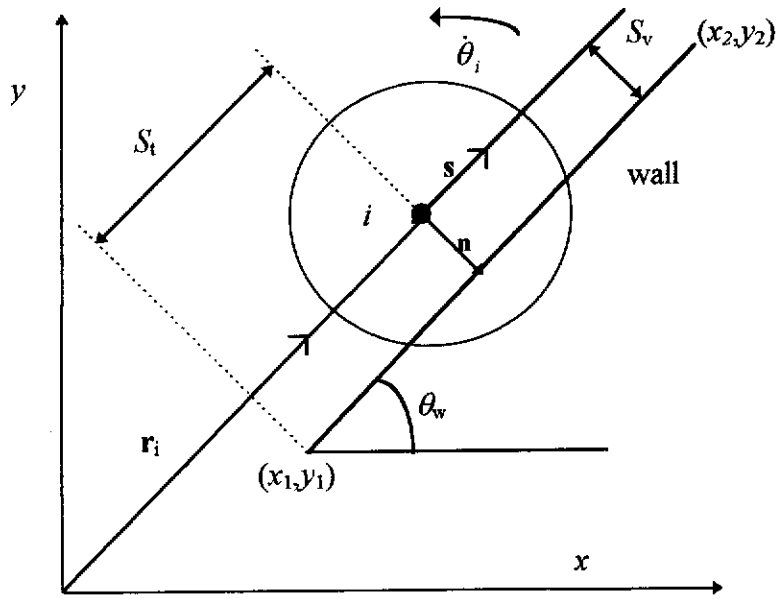

Figure 3.4 Particle-wall contact

where $\boldsymbol{F}_{ijn}$ is the normal force and $\boldsymbol{F}_{ijs}$ is the shearing force acting on the particle, **n** and **s** are unit vectors in the normal and shear directions of the contact plane as shown in figure 3.5.

Various models have been proposed for the calculation of $F_{ijn}(t)$ and $F_{ijs}(t)$, such as those by Zheng and Hill (1996) and Langston et al (1995). In the present study, the particle-particle interaction is modelled as a dynamic process and a viscoelastic model as shown in figure 3.6 is used to describe this process. The interaction forces developed between the particle pair in contact are calculated based on their relative movement. The interaction force in normal direction **n**

consists of an elastic contribution and a viscous damping contribution. The elastic contribution can be determined by using Hertz's contact formula

$$f_{ijn}^{e}(t) = -\left(\frac{\pi G}{(1-\nu)\left[2\ln\left(\gamma / f_{ijn}^{e}(t)\right)-1\right]}\right)\delta_{ijn}(t) \quad , \tag{3.9}$$

where G and ν are the shear modulus and Poisson's ratio of the material. To simplify the computation we can approximate the elastic force components by Hooke's law with an appropriately chosen stiffness, K_n. The viscous component is assumed to be proportional to the relative normal velocity of the particle pair in contact, i.e

$$f_{ijn}^{d}(t) = -\lambda_n m\dot{\delta}_{ijn}(t) \quad , \tag{3.10}$$

where λ_n is the contact damping coefficient.

The force in the shear direction s is modelled as viscoelastic below the friction limit and frictional at the frictional limit given by Mohr-Coulomb law,

$$f_{ijs\ \max} = c + \mu f_{ijn} \quad , \tag{3.11}$$

where c and μ are cohesive strength and friction coefficient of the material. Thus the shear force can be determined by

$$f_{ijs}(t) = -sign\left[\delta_{ijs}(t)\right]\min\left\{K_s\left|\delta_{ijs}(t)\right|,\ \ c+\mu f_{ijn}^{e}(t)\right\} - \lambda_s m\dot{\delta}_{ijs}(t) \quad , \tag{3.12}$$

Similar formulae can be derived for the calculation of particle-wall interaction forces.

3.4 Calculation of Contact Forces

3.4.1 Particle-particle contact

Consider the contact of two discs, *i* and *j*, as shown in figure 3.5. For convenience of analysis, we introduce the following notation

$\mathbf{r}_i$, $\mathbf{r}_j$ = position vectors of the centres of discs *i* and *j*,

$\mathbf{r}_i = (x_i, y_i)$, $\mathbf{r}_j = (x_j, y_j)$.

$\mathbf{v}_i$, $\mathbf{v}_j$ = velocity vector of the centres of particles *i* and *j*,

$\dot{\theta}_i, \dot{\theta}_j$ = angular velocities of particles *i* and *j*, taken positive in counter clockwise direction.

$\mathbf{n}$ = unit vector pointing from the centre of *i* to the centre of *j*, that is

$\mathbf{n} = ((\mathbf{r}_j - \mathbf{r}_i)/(|\mathbf{r}_j - \mathbf{r}_i|) = (\cos\alpha, \sin\alpha)$

$\mathbf{s}$ = unit vector obtained by a counterclockwise rotation of $\mathbf{n}$ through 90°, i.e

$\mathbf{s} = (-\sin\alpha, \cos\alpha)$

The relative velocity at the contact point is defined as the relative velocity of point *i* with respect to *j*, i.e

$$\mathbf{v}_{i/j} = (\dot{\mathbf{r}}_i - \dot{\mathbf{r}}_j) + R(\dot{\theta}_i + \dot{\theta}_j)\mathbf{s} \qquad (3.13)$$

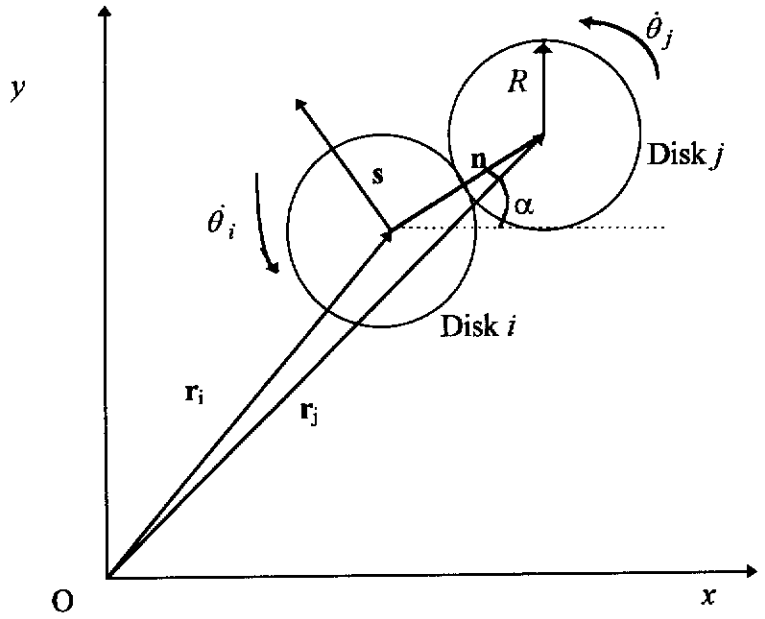

Figure 3.5 Particle pair in contact

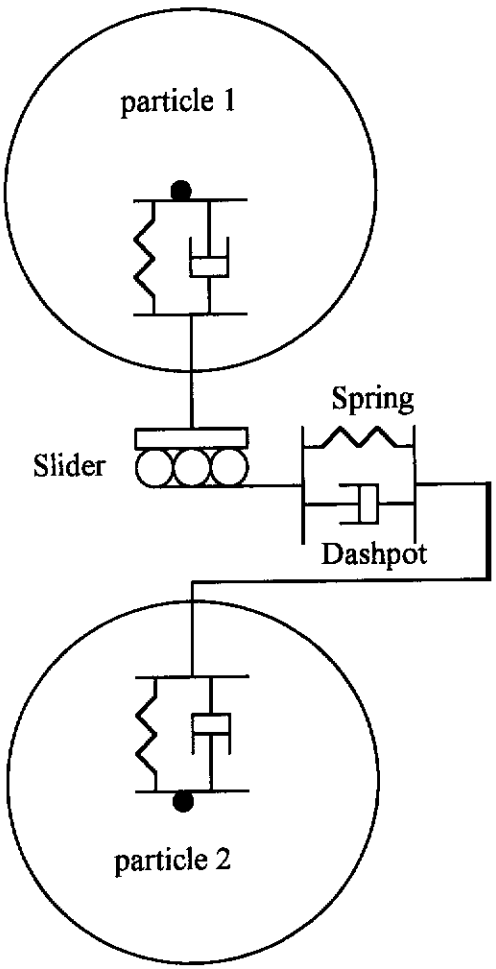

Figure 3.6 The viscoelastic contact model

The relative velocities in the normal and tangential directions are the projections of $\mathbf{v}_{i/j}$ on the normal direction and tangential direction respectively and are given by

$$v_n = \mathbf{v}_{\mathbf{i/j}}.\mathbf{n} = (u_i - u_j)\cos\alpha + (v_i - v_j)\sin\alpha \quad , \tag{3.14}$$

$$v_s = \mathbf{v}_{\mathbf{i/j}}.\mathbf{s} = -(u_i - u_j)\sin\alpha + (v_i - v_j)\cos\alpha + R(\dot{\theta}_i + \dot{\theta}_j) \quad . \tag{3.15}$$

These relative displacement rates are then input into the contact force model to calculate the increment of contact forces. Thus, the total contact force in the normal and tangential directions are respectively

$$F^N{}_n = F^{N-1}{}_n + \Delta F_n \quad , \tag{3.16}$$

$$F^N{}_t = F^{N-1}{}_n + \Delta F_s \quad . \tag{3.17}$$

The force in the tangential direction is subject to the yielding condition as described by (3.12).

The x and y components of the contact forces and the moment acting on particle i are then calculated as

$$\begin{bmatrix} F_x^N \\ F_y^N \\ M \end{bmatrix} = \begin{bmatrix} \cos\alpha & \sin\alpha \\ \sin\alpha & \cos\alpha \\ 0 & -R \end{bmatrix} \begin{bmatrix} F_n^N \\ F_s^N \end{bmatrix} . \tag{3.18}$$

3.4.2 Particle-wall contact

Consider the particle-wall contact as shown in figure 3.4. Let

$\mathbf{r}_i$ = position vector of the centre of disk *i*, namely

$\mathbf{r}_i = (x_i, y_i)$

$\dot{\mathbf{r}}_i$ = velocity vector of the centre of disk *i*, namely

$\dot{\mathbf{r}}_i = (u_i, v_i)$

$\dot{\theta}_i$ = angular velocity of *i* taking positive in counter clockwise direction

$\mathbf{n}$ = unit vector pointing from the centre of disk *i* to the point of contact with the wall, namely

$\mathbf{n} = (\sin\theta_w, -\cos\theta_w)$

$\mathbf{s}$ = unit vector obtained by a counterclockwise rotation of $\mathbf{k}$ through 90°, namely

$\mathbf{s} = (\cos\theta_w, \sin\theta_w)$

Then, the relative velocity $\mathbf{v}_{i/w}$ of the point of contact is defined as the relative velocity of particle *i* with respect to the wall, namely

$$\mathbf{v}_{i/w} = \dot{\mathbf{r}}_i - \dot{\mathbf{r}}_W + R\dot{\theta}_i\mathbf{s} + s_t\dot{\theta}_W\mathbf{n} \quad . \tag{3.19}$$

The relative velocities in the normal and tangential direction are respectively the projection of $\mathbf{v}_{i/w}$ on the normal and tangential direction respectively, namely

$$\delta_n = \mathbf{v}_{i/w}.\mathbf{n} = (u_i - u_w)\sin\theta_w - (v_i - v_w)\cos\theta_i + s_t\dot{\theta}_i \quad ,$$

$$\delta_t = \mathbf{v}_{i/w}.\mathbf{s} = (u_i - u_w)\cos\theta_w + (v_i - v_w)\sin\theta_i + R\dot{\theta}_i \quad . \tag{3.20}$$

These relative velocities are then used in the contact force model to calculate the increment of contact forces and consequently F_n^N and F_s^N. Therefore the x and y components of the contact force and the moment acting on particle i are

$$\begin{bmatrix} F_x \\ F_y \\ M_a \end{bmatrix} = \begin{bmatrix} -\sin\theta_w & -\cos\theta_w \\ \cos_w & -\sin\theta_w \\ 0 & -R \end{bmatrix} \begin{bmatrix} F_n^N \\ F_s^N \end{bmatrix} \quad . \tag{3.21}$$

The force and moment on the wall are thus given by

$$\begin{aligned} (F_x)_w &= -F_x^N \quad , \\ (F_y)_w &= -F_y^N \quad . \end{aligned} \tag{3.22}$$

3.5 Particle Motion

The equations governing the motion of each individual particle, i, is the principle of linear momentum and the principle of angular momentum, namely

$$m\ddot{\mathbf{r}}_i(t) + \lambda m\dot{\mathbf{r}}_i(t) = \mathbf{F}_i(t), \qquad I\ddot{\theta}_i(t) + \lambda I\dot{\theta}_i(t) = M_i(t), \quad (i = 1, N) \tag{3.23}$$

where M and I are the mass and moment of inertia of the particle, λ is a damping coefficient, $\mathbf{F}_i(t)$ and $M_i(t)$ are the total force and moment acting on particle i, $\mathbf{r}_i(t)$ is the position vector of the center of disc i and $\dot{\theta}_i(t)$ denotes the rotating speed of disc i, the superimposed dot indicates differentiation with respect to time t.

Let $\mathbf{v}_i = \dot{r}_i$, $\omega = \dot{\theta}_i$, we have

$$\begin{cases} \dot{\mathbf{r}}_i = \mathbf{v}_i \ , \\ \dot{\theta}_i = \omega_i \ , \\ \dot{\mathbf{v}}_i(t) + \lambda \mathbf{v}_i(t) = \dfrac{\mathbf{F}_i(t)}{m_i} \ , \\ \dot{\omega}_i(t) + \lambda \omega_i(t) = \dfrac{M_i(t)}{I_i} \ , \end{cases} \qquad i = 1,2,...N \ , \tag{3.24}$$

which constitute a system of $4N$ first order ordinary differential equations, namely

$$\begin{aligned} &\frac{d\mathbf{z}(t)}{dt} = \mathbf{v}(t) \ , \\ &\frac{d\mathbf{v}(t)}{dt} + \lambda \mathbf{v}(t) = \mathbf{P}\left[\mathbf{x}(t), \mathbf{v}(t)\right] , \end{aligned} \tag{3.25}$$

where

$$\mathbf{z}(t) = \left[\mathbf{r}_1(t), \theta_1(t), ... \mathbf{r}_N(t), \theta_N(t)\right]^T ,$$

$$\mathbf{P}(x,v) = \left[\frac{\mathbf{F}_1(\mathbf{x},\mathbf{v})}{m_1}, \frac{M_1(\mathbf{x},\mathbf{v})}{I_1}, ..., \frac{\mathbf{F}_N(\mathbf{x},\mathbf{v})}{m_N}, \frac{M_N(\mathbf{x},\mathbf{v})}{I_N}\right]^T .$$

(3.26)

From equation $(3.25)_2$, on using the centered difference formula at time t^n and approximating $\mathbf{v}^n$ by $\frac{1}{2}$ $(\mathbf{v}^{n-½} + \mathbf{v}^{n+½})$, we have

$$\mathbf{v}^{n+½} = \alpha \, \mathbf{v}^{n-½} + \beta \mathbf{P}^n \tag{3.27}$$

where the superscript n-½ refers to a quantity evaluated at the instant of time t_n-½Δt and

$$\alpha = \left(1 - \frac{\lambda \Delta t}{2}\right)\left(1 + \frac{\lambda \Delta t}{2}\right)^{-1}, \quad \beta = \Delta t \left(1 + \frac{\lambda \Delta t}{2}\right)^{-1} \ . \tag{3.28}$$

A further application of the centered difference formula to $(3.25)_1$ at time $t_n+\frac{1}{2}\Delta t$ yields

$$\mathbf{z}^{n+1} = \mathbf{z}^n + \mathbf{v}^{n+\frac{1}{2}}\Delta t \quad . \tag{3.29}$$

3.6 Calculation of Wall Pressures

We choose an element of length l on the boundary (wall) then analyse the force exerted by the granular material on the wall. Assuming that within l there are m contact points c_1, c_2 ... c_m and the contact force at c_p is $\mathbf{F}_p^c = (F_{px}^c, F_{py}^c)$, then we define the average contact force on l by

$$\mathbf{p} = \frac{1}{l}\sum_{i=1}^{m}\mathbf{F}_i^c \quad . \tag{3.30}$$

The normal and tangential components are respectively

$$p_n = \frac{1}{l}\sum_{i=1}^{m}\left(\mathbf{F}_i^c n_i\right) \quad ,$$

$$p_t = \frac{1}{l}\sum_{i=1}^{m}\left(\mathbf{F}_i^c t_i\right) \quad , \tag{3.31}$$

where (n_i, t_i) represents a unit vector along the direction of $\mathbf{F}_i^c$ as shown in figure 3.7.

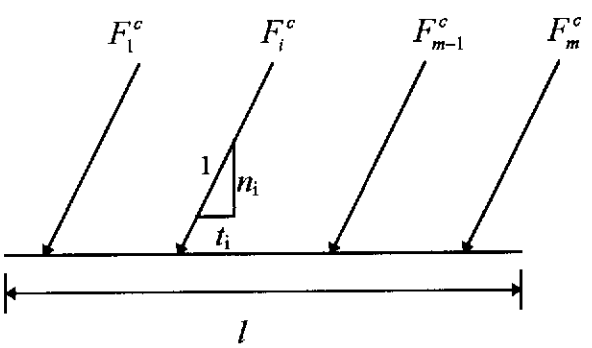

Figure 3.7 : Contact forces acting on the wall

3.7 Calculation of Stresses in Granular Materials

3.7.1 Static case

Consider a volume V of granular material with boundary S. Let σ_{ij} be the stress tensor, **n** be the outward unit normal of S, **F** be boundary tractions. Then under the static equilibrium condition, if body forces can be neglected, we have

$$\sigma_{ij,i} = 0 \quad \text{in } V \quad , \tag{3.32}_1$$

$$\sigma_{ij} n_j = F_i \quad \text{on } S \quad , \tag{3.32}_2$$

where we have used the index notation with repeated index representing summation.

The average stress tensor in V is defined as

$$\sigma_{ij} = \frac{1}{V}\int_V \sigma_{ij} dV \quad . \tag{3.33}$$

The integral becomes a summation for a particulate material because stresses exist only within particles. Thus, assuming that there are N particles in V, we have

$$\sigma_{ij} = \frac{1}{V}\sum_{p=1}^{N} \sigma_{ij}^{p} V^{p} \quad , \tag{3.34}$$

where V^p is the volume of the p^{th} particle. In the same way the average stress tension within particle p is defined as

$$\sigma_{ij}^{p} = \frac{1}{V^{p}}\int_{V^p} \sigma_{ij} dV \quad .$$

As

$$\sigma_{ij} = \sigma_{ik}\delta_{jk} = (\sigma_{ik}x_j)_{,k}$$

we have

$$\sigma_{ij}^{p} = \frac{1}{V^{p}} \int_{V^{p}} (\sigma_{ik}x_j)_{,k}\, dV \tag{3.35}$$

where in deriving above formulas, we have used equation (3.33).

Now from the divergence theorem, we have

$$\sigma_{ij}^{p} = \frac{1}{V^{p}} \int_{S_p} (\sigma_{ik}x_j) n_k ds \quad , \tag{3.36}$$

where $\mathbf{n} = (n_1, n_2)$ is the unit normal direction of S_p. Thus we have

$$\sigma_{ij}^{p} = \frac{1}{V^{p}} \int_{S_p} (F_i x_j) ds \quad , \tag{3.37}$$

which becomes a sum by noting that the surface is discrete. Therefore

$$\sigma_{ij}^{p} = \frac{1}{V^{p}} \sum_{c=1}^{m} x_i^c F_j^c \quad . \tag{3.38}$$

where m is the number of contact points on S_p and x_i^c is the coordinate of the contact point c. Hence, the average stress in V, namely σ_{ij}, can be determined by substituting (3.38) into (3.34), i.e.

$$\sigma_{ij} = \frac{1}{V} \sum_{p=1}^{N} \sum_{c=1}^{m} x_i^c F_j^c \quad .$$

3.7.2 Dynamic case

For the dynamic case, the equation of motion is

$$\rho \frac{dv_i}{dt} = \sigma_{ik,k} + \rho g_i \quad , \tag{3.39}$$

which gives rise to

$$\sigma_{ik,k} = \rho \frac{dv_i}{dt} - \rho g_i \quad . \tag{3.40}$$

Following the procedure used in the derivation of the average stress for the static case, we have for the dynamic case,

$$\sigma_{ij}^p = \frac{1}{V^p} \int_{V^p} \sigma_{ij} dV$$

$$= \frac{1}{V^p} \left\{ \int_{S_p} \left(\sigma_{ik} x_j \right)_{,k} dV \; - \rho \int_{V^p} \left(\frac{dv_i}{dt} - g_i \right) x_j dV \right\}$$

$$= \frac{1}{V^p} \left\{ \int_{S_p} \sigma_{ik} n_k x_j dS - \rho \int_{V^p} \left(\frac{dv_i}{dt} - g_i \right) x_j dV \right\}$$

$$= \frac{1}{V^p} \left\{ \int_{S_p} F_i x_j dS - \rho \int_{V^p} \left(\frac{dv_i}{dt} - g_i \right) x_j dV \right\}$$

$$= \frac{1}{V^p} \left\{ \sum_{c=1}^{M} F_i^c x_j^c - \rho V^p x_j \left(\frac{dv_i^p}{dt} - g_i \right) \right\}. \tag{3.41}$$

Thus for volume V,

$$\sigma_{ij} = \frac{1}{V} \left\{ \sum_{p=1}^{M} \sum_{c=1}^{M} F_i^c x_j^c - \rho \sum_{p=1}^{N} V^p x_j \left(\frac{\partial v_i^p}{\partial t} - g_i \right) \right\}. \tag{3.42}$$

For circular particles, we have

$$x_i^c = x_i^p + R^p n_i^c \quad ,$$

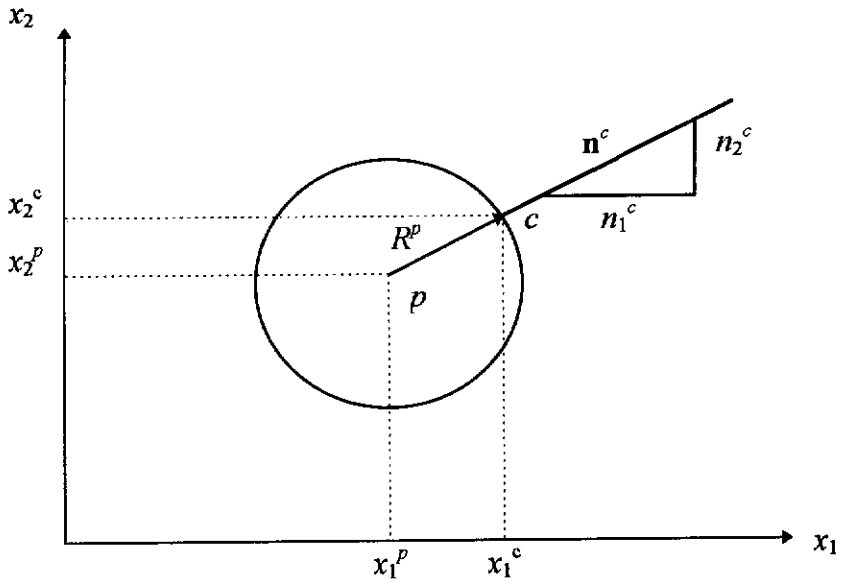

Figure 3.8. Diagram showing the relation between x_i^p and x_i^c.

where x_i^p is the coordinates of the centre of particle p, R^p is the radius of particle p, x_i^c is the coordinates of the contact point c and $\mathbf{n}^c = (n_1^c, n_2^c)$ denotes a unit vector from p to c as shown in figure 3.8. Thus, we have

$$\sigma_{ij} = \frac{1}{V}\left[\sum_{p=1}^{N}\sum_{c=1}^{M}\left(x_i^p + R^p n_i^c\right)F_j^c - \rho\sum_{p=1}^{N}V^p x_i^p\left(\frac{\partial v_j^p}{\partial t} - g_j\right)\right] \quad . \tag{3.43}$$

Noting that

$$\sum_{c=1}^{M}\left(x_i^p F_j^c\right) - \rho V^p x_i^p\left(\frac{\partial v_j^p}{\partial t} - g_j\right) = x_i^p\left\{\sum_{c=1}^{M}F_j^c - \rho V^p\left(\frac{\partial v_j^p}{\partial t} - g_j\right)\right\} \approx \mathbf{0} \quad , \tag{3.44}$$

we have

$$\sigma_{ij} = \frac{1}{V}\sum_{p=1}^{N}R^p\sum_{c=1}^{M}n_i^c F_j^c \quad . \tag{3.45}$$

The stress tensor may be split into two parts, $\sigma_{ij}(n)$ due to normal forces and $\sigma_{ij}(s)$ due to shear forces. Let $F_i(n)$ and $F_i(s)$ represent respectively the projections of normal and shear forces on the x_i axis as shown in figure 3.9, namely

$$F_i = F_i(n) + F_i(s) \,. \tag{3.46}$$

Then,

$$F_i(n) = (F_n)n_i = (F_k n_k)n_i \quad , \quad F_i(s) = F_s t_i = (F_K t_K)t_i \quad . \tag{3.47}$$

Therefore, from (3.46), we have

$$\sigma_{ij}(n) = \frac{1}{V}\sum_{p=1}^{N} R^p \sum_{c=1}^{M} n_i^c (F_k^c n_k^c n_j^c) = \frac{1}{V}\sum_{p=1}^{N} R^p \sum_{c=1}^{M} (n_i^c F_k^c n_k^c n_j^c) \quad ,$$

$$\sigma_{ij}(s) = \frac{1}{V}\sum_{p=1}^{N} R^p \sum_{c=1}^{M} n_i^c (F_j^c(s)) = \frac{1}{V}\sum_{p=1}^{N} R^p \sum_{c=1}^{M} (n_i^c F_k^c t_k^c t_j^c) \quad , \tag{3.48}$$

and

$$\sigma_{ij} = \sigma_{ij}(n) + \sigma_{ij}(s) \quad .$$

3.8 Simulation Program Development

Based on the algorithms described in the previous sections for searching particle contacts, computing contact forces and updating particle velocities and positions, a computer program has been developed for analysing the flow behaviour of particles in silos. The program basically consists of three units

- a pre-processing unit

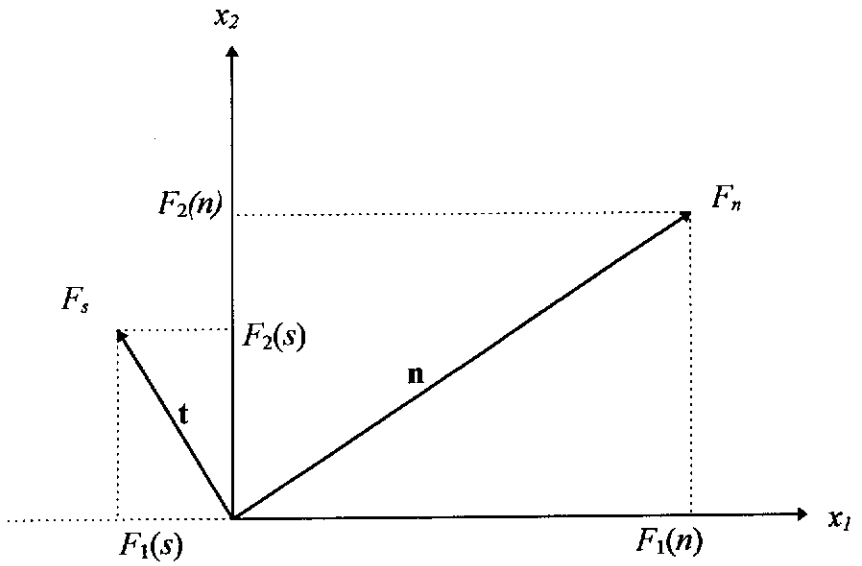

Figure 3.9. Diagram showing the relationship among F_i, $F_i(n)$ and $F_i(s)$

- a simulation unit
- a post-processing unit

3.8.1 Pre-processing unit

The input parameters defining the problem to be studied are specified in the pre-processing unit. The parameters required include physical properties of the granular material under consideration, initial conditions and boundary conditions.

The initial conditions include the initial positions and velocities of all particles and the geometry of the silo under consideration. This information can be either read in from an input file or calculated from a supplementary subroutine.

3.8.2 Simulation unit

The simulation unit is the main part of the program, which is called each time to determine the state of the particle system at a new instant of time. It consists of a search for all existing contacts, calculation of interparticle forces at all contacts from the force-displacement law, integration of equations of motion to obtain new positions and velocities of all particles, application of specific boundary conditions and updating of stress, wall pressures and velocities. This program unit is called thousands of times as the simulation proceeds.

3.8.3 Post-processing unit

This program unit is designed to output, in both table and graphic forms, the results of interest in the flow analysis. The flow pattern of material and the wall pressure distributions can be shown on the screen of monitors by calling this program unit.

3.8.4 Program structure

Figure 3.10 shows the flow chart of the program developed. The overall program structure and the relationships of the subroutines are shown in figure 3.11. The functions carried out by the subroutines of the program are shown in table 3.1.

Table 3.1. Program subroutines

Subroutine Name	Function
readdat	Read input data from a file
setwin	Set-up a window on monitor
wallelsetup	Create a rectangular grid
setup	Set up initial conditions (initial position and velocity)
neighbour	Detect contacts
simulator	
force	Determine contact forces
fppcontact	Determine particle-particle contact forces
fpwcontact	Determine particle-wall contact forces
wallpres	Calculate wall pressures
update	Calculate new position and velocity of every particle
output	Provide output data to screen
flowpic, flowpicture	Display granular flow on screen

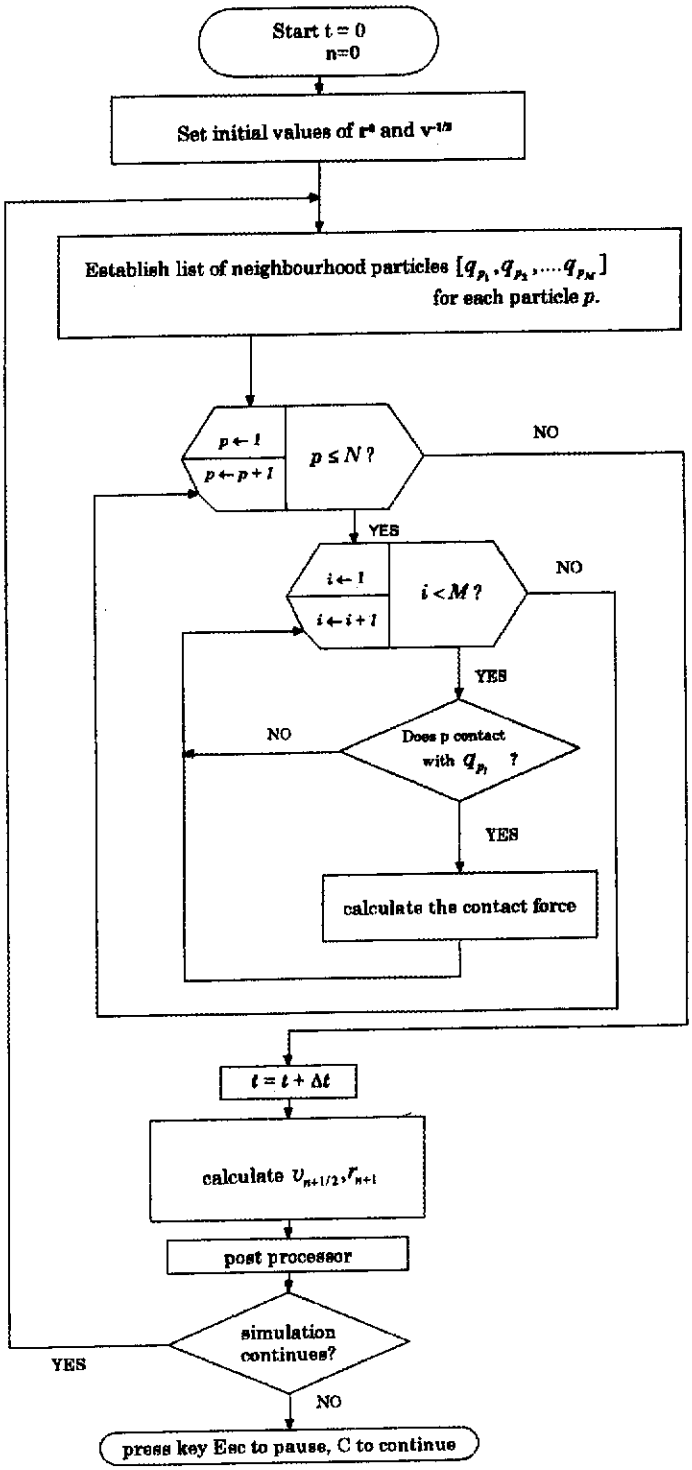

Figure 3.10 Program flow chart

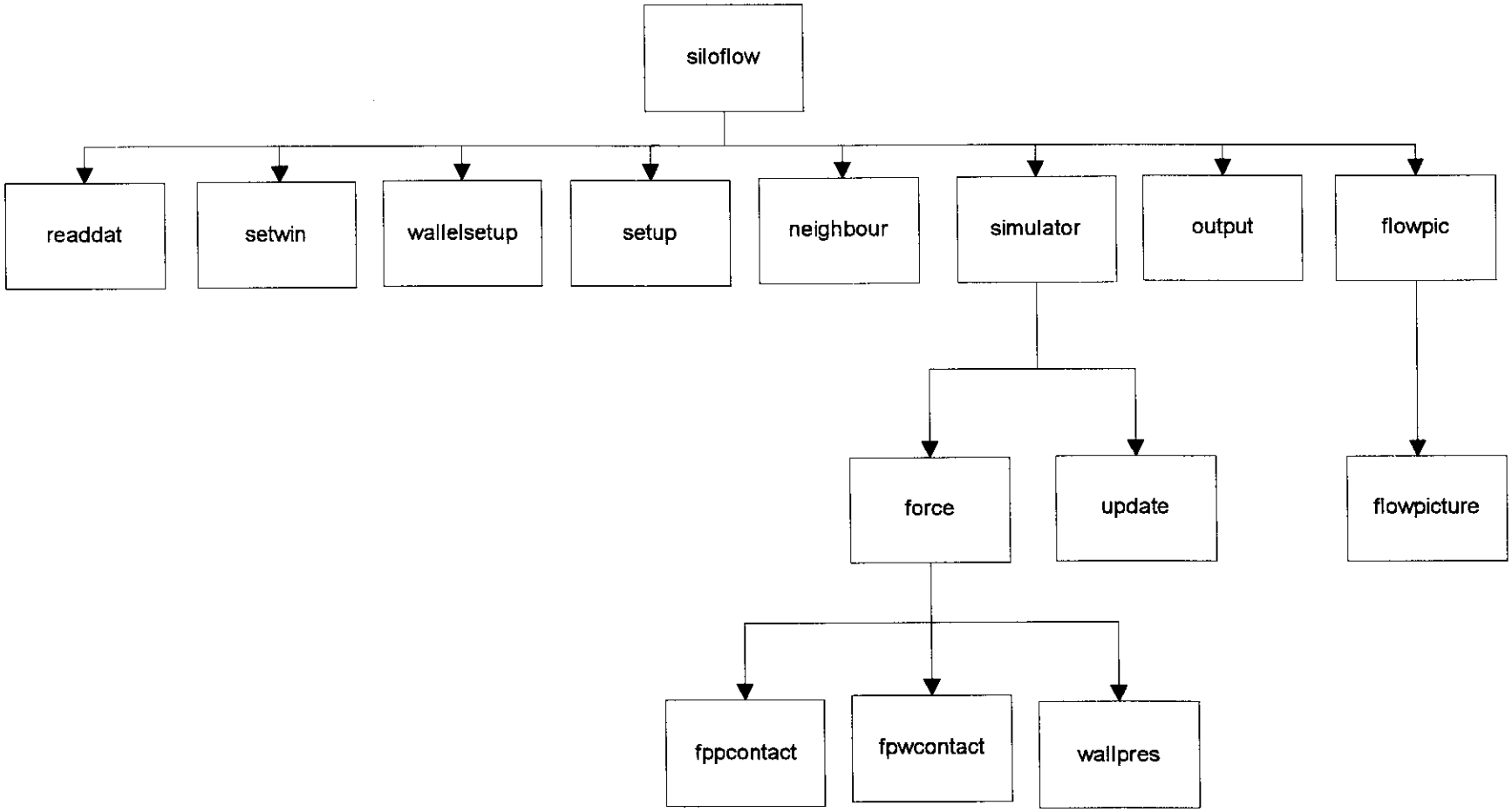

Figure 3.11 Program structure chart

3.9 Summary

An efficient discrete dynamic model has been developed and implemented for the simulation of granular flows in silos. The calculation of pressures on silo walls, velocity and stress fields in granular materials has been mathematically formulated. The developed model thus provides a means for investigating the flow behaviour of granular materials in silos.

Chapter 4

FLOW BEHAVIOUR AND WALL PRESSURES DURING STORAGE AND DISCHARGE

4.1 General

The difficulty in arriving at meaningful data from experiments with granular materials is to attempt not to influence or corrupt the data gathered. It is difficult to produce nonintrusive testing equipments to measure parameters such as velocity and granular temperature. It is therefore useful to produce computer simulation data and to compare these against experimental data. The use of computer simulation can assist in at least three ways. Firstly, the models can suggest assumptions for the theoretical models and to support, or deny, existing models. A second objective is to produce models of the mechanics of particle to particle and particle to wall interactions. Another objective is to examine additional forces or structures within the granular material, for example the microstructural activity (Campbell and Brennen, 1985). In this chapter, the method developed and presented in chapter 3 will be used to study the flow of granular materials in silos. Emphasis is given to the investigation of flow patterns,

wall pressure distributions and the influence of various system parameters on the flow behaviour. In the following section, we study in detail the flow pattern and pressure distribution for a typical silo-granular material system in detail. In section 4.3, we investigate the influence of wall friction, silo geometry and particle size on silo wall pressures and flow patterns.

4.2 Simulation of Filling and Discharge process

4.2.1 Simulation set-up

The geometry of the silo under consideration is shown in figure 4.1. To simulate the actual silo filling process, the model granules are introduced into the top of the silo gradually and are allowed to fall under gravity into the silo. During the filling stage, the outlet of the silo is closed. Thus, due to frictional and damping forces, the assembly eventually comes to rest at the base of the silo. Once the silo is fully filled with particles and a near steady-state condition has been achieved, the outlet of the silo is opened and the particles are allowed to flow out of the silo under gravity. If the level of material in the silo is to be maintained constant, a new particle is filled into the silo from its top once a particle completely flows out of the silo.

4.2.2 Simulation Input

Input values for a number of parameters are required for the simulation. Table 4.1 lists the values used in the current simulation.

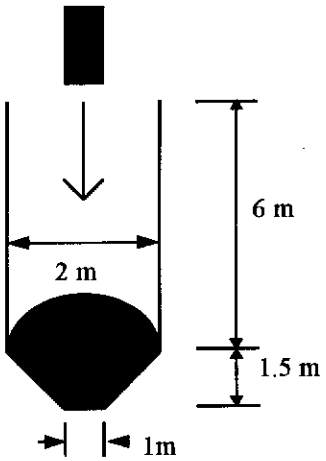

Figure 4.1 : Silo geometry

Table 4.1. Simulation input values

Friction coefficients:	
particle-particle	0.6
particle-wall	0.4
Particle radius	0.04 m
Contact damping coefficient	$\lambda_n = \lambda_s = 5$
Global damping coefficient	$\lambda = 0$
Elastic constants	K_n=1000 kN/m, K_s=800kN/m
Time interval	0.00003 sec
Material density	2000 kg/m^3

4.2.3 Flow patterns and wall pressure distributions

Figure 4.2 shows the flow patterns of the granular material in the silo and the distribution of pressure on silo walls at different instants of time, with t=0 representing the start of discharge of materials from the outlet.

Mass flow can be seen to occur in the entire silo. It is possible to identify three flow zones, these being the pipe zone, the pipe feed zone and the plug flow zone. In the region of transition from the silo to the hopper, the particle moving direction changes sharply from vertical to a direction parallel to the hopper inclined wall, resulting in high pressure at this point as shown in figure 4.2.

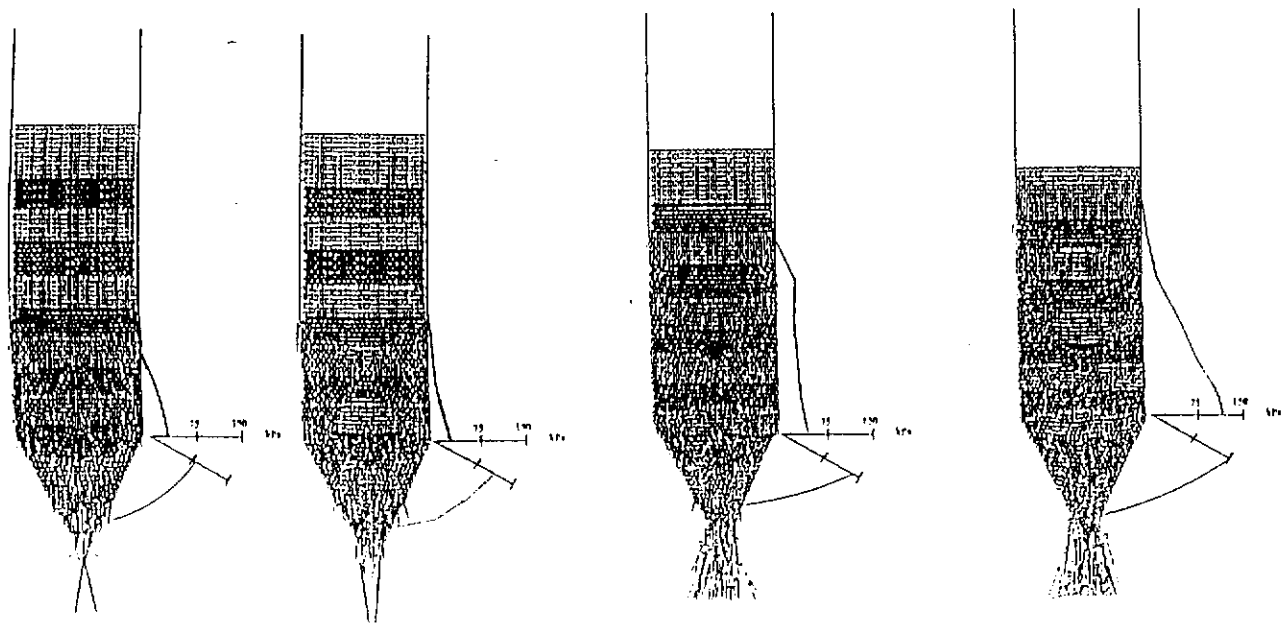

Figure 4.2. Flow patterns and pressures for conical bottomed silo

It can also be noted that there is a large increase in wall pressure in the transition zone from vertical flow to the conical hopper region. The wall pressure reaches the maximum at the transition point and decreases towards the outlet. This result is generally in agreement with existing experiment results.

4.3 Numerical Investigations

4.3.1 Effect of wall friction

To investigate the effect of wall friction on the flow of granular materials, a series of test simulations were run. The methodology was to maintain other parameters of the simulation the same while varying the wall friction coefficient (μ_w). The trials were conducted using the parameter values shown in table 4.1, except the values of μ_w was changed from 0 to 0.6.

Figure 4.3 shows the wall pressure distribution for different value of μ_w. It can be noted that as the wall friction coefficient increases, the normal pressure on the walls of the silo decreases, at each point down the silo.

4.3.2 Effect of internal friction

To investigate the effects of internal friction, the angle of internal friction was varied from 0 to 31 degrees. Figure 4.4 shows the distributions of pressures on silo walls under both static and discharging conditions. For ϕ=0 and μ_w=0, the

normal pressure is reasonably close to the hydrostatic pressure as would be expected. On discharge, the wall pressure on the region adjacent to the outlet is

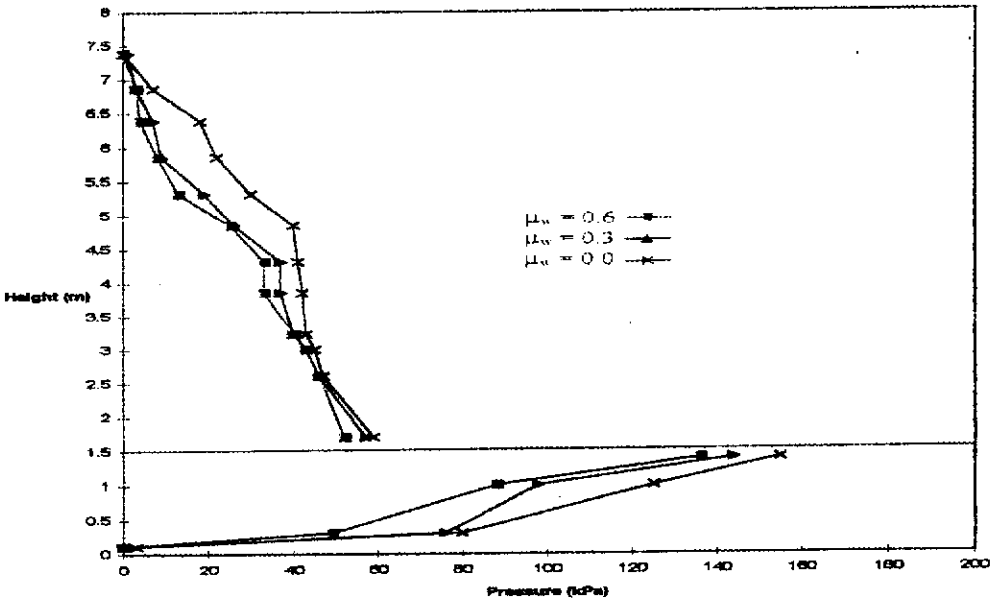

Figure 4.3. Wall pressure distributions for different value of μ_w.

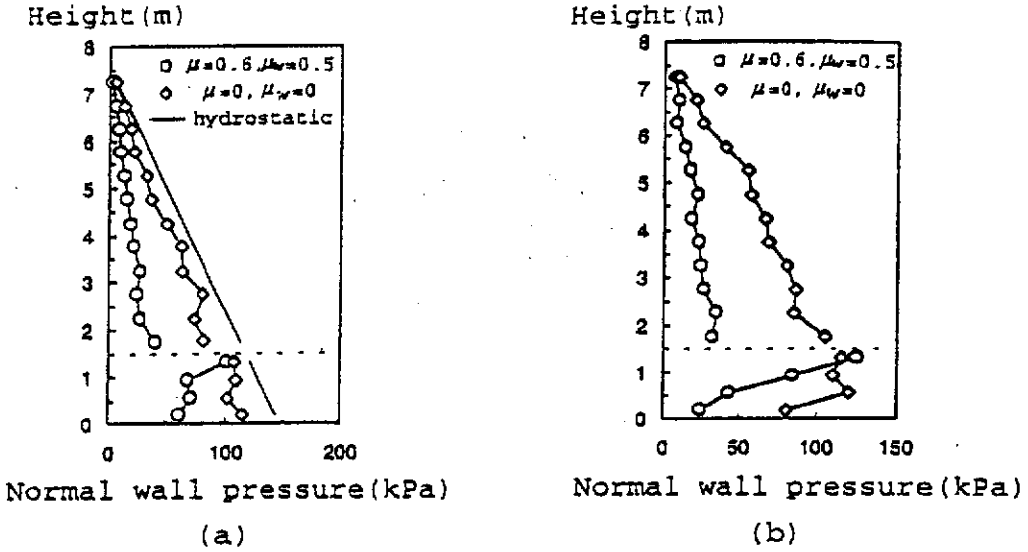

Figure 4.4. Distribution of normal pressure on silo wall at (a) static state and (b) silo emptying state.

slightly lower than that in the static case. This decrease of pressure can be attributed to the dilation of the particle zone in the outlet region during flow.

For ϕ=31 degrees and μ_w=0.5, the filling normal pressure is significantly lower than the hydrostatic pressure, which agrees with existing silo pressure theories. During the process of discharge, a high pressure zone on the transition between hopper and vertical bin wall is detected, which agrees with other numerical results such as those derived using the finite element method.

4.3.3 Effect of silo geometry

Various silo geometries were tested to ascertain their effects on flow characteristics. The silo geometries are shown in figure 4.5. The heights referred to in the following discussion are based on distance measured from the bottom or the lowest point of the silo.

Figure 4.6 shows the flow patterns of material through a conical bottomed silo, a flat bottomed silo and a sloping bottomed silo. It can be noted that in the conical bottomed silo there is a developing flow pattern down the centre axis of the silo, where greater movement is apparent. Although this has characteristics of a funnel flow pattern, overall there appears to be a mass flow of the material. Along the sides of the silo and down the hopper section sides, movement of particles are clearly visible. In the case of the flat bottomed silo, there is a similar axial flow

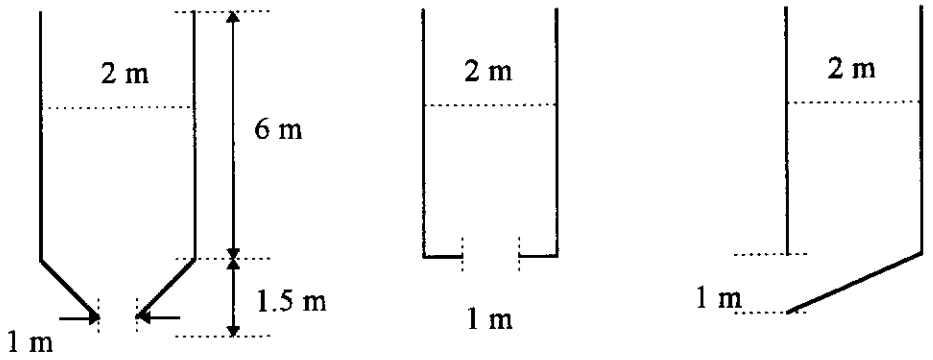

Figure 4.5 Silo geometries

pattern. There are clear stagnant zones in either side of the exit orifice and the size of this region was found to depend on a number of input parameters, including friction coefficients and particle size. In the sloping bottomed silo the main flow is along an axial line to the right of centre, away from the discharge side.

Figures 4.7 shows the pressure variations of a conical bottomed silo during discharge of the silo. It can be noted that the pressure on vertical bin wall is fairly constant, except a slight increase on the area near the bin-hopper transition. There is a large increase in pressure at the transition zone and a decrease of pressure near the outlet. The pressure on the cone section is significantly higher than that on the vertical wall. The transition point from vertical wall to hopper wall is marked by a horzontal line as shown in the figure. The predicted pressure distribution is consistent with existing experimental findings.

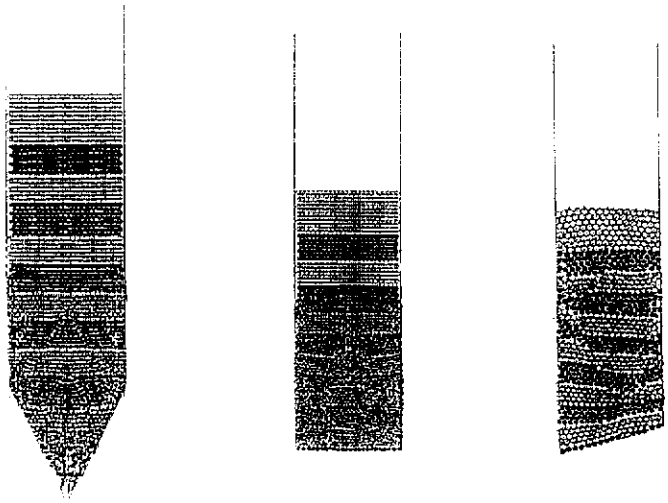

Figure 4.6. Flow patterns in conical, flat and sloping bottomed silos.

Figure 4.8 shows the pressure profile for a flat bottomed silo. When the outlet is opened, granular material starts to flow out of the outlet. The pressure on the wall near the bottom decreases, which may be attributed to the loosening of material in the region near the outlet. It can also be noted that, there also exists a region on the wall where the pressure on flow conditions is higher than that on static conditions.

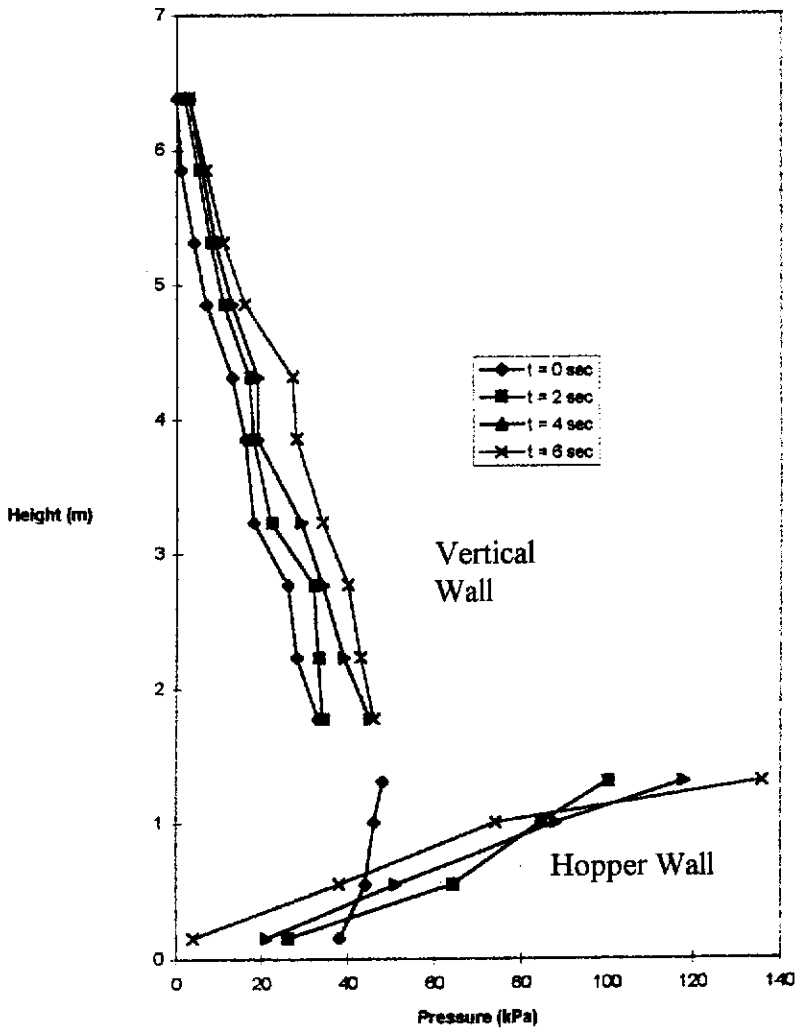

Figure 4.7. Pressure distribution on the wall of a conical silo .

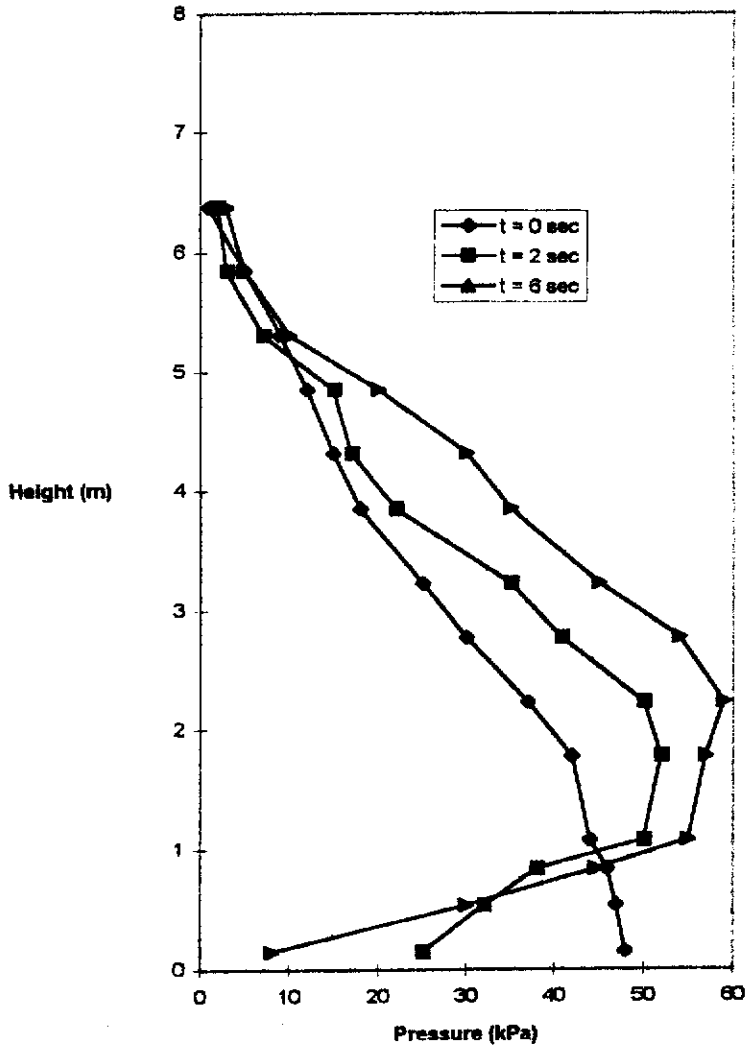

Figure 4.8. Pressure distribution on the wall of a flat bottomed silo.

Figure 4.9 shows the pressure distribution on the wall (left hand side) of the sloping bottomed silo as shown in figure 4.5. The static pressure profile is similar to that of the pressure on other type of silos. When the outlet is opened, the pressure on the outlet is reduced from the static pressure to zero and the granular

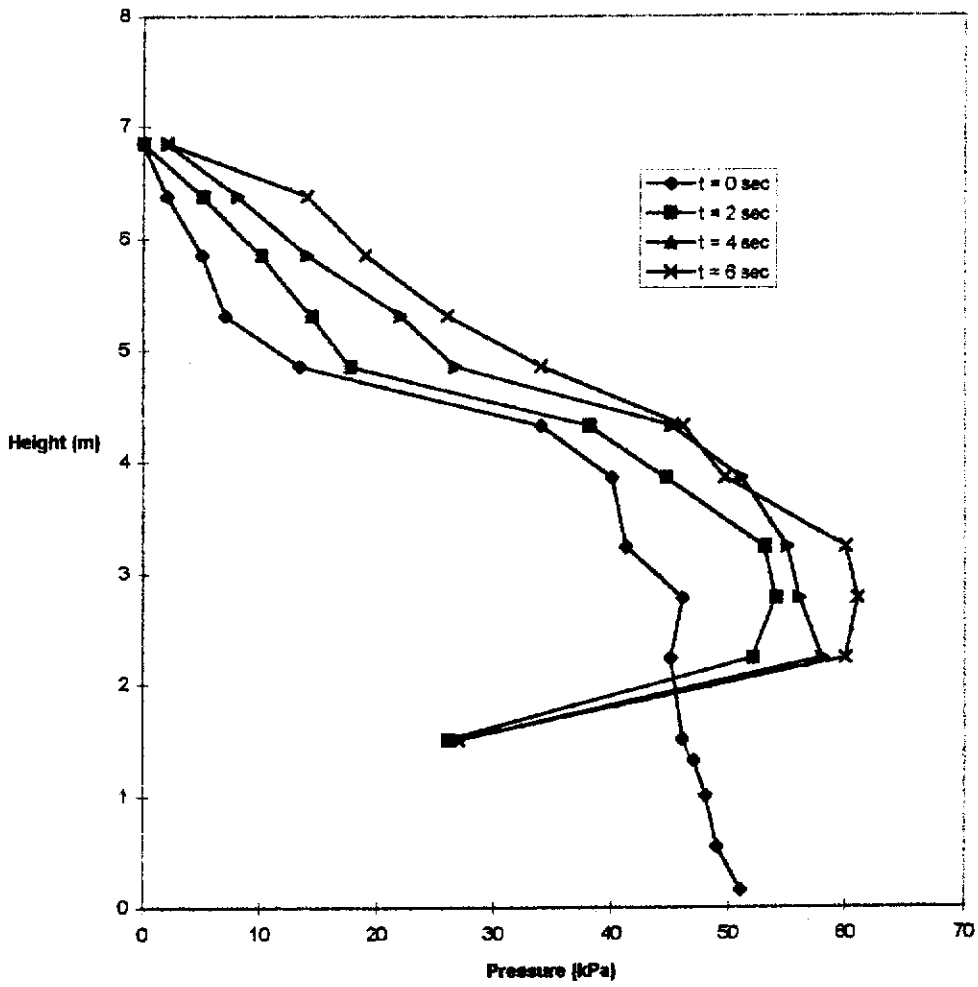

Figure 4.9. Pressure distribution on the wall of a sloping bottomed silo.

material starts to flow out of the outlet. There is a pressure decrease in the side wall area near the outlet. It can also be noted that there exists a region where the pressure on flow conditions is larger that on static conditions. The numerical results produced suggest that pressure exerted by granular material on the hopper wall is higher than the pressure on the vertical wall of a flat bottomed silo.

However, the pressure on the bottom of the flat bottom silo is expected to be very high.

Figure 4.10, provides a comparison of pressures on various silos at various heights during discharge. From the table in this figure, it can be seen that the conical bottomed silo has the largest pressure on the wall compared to other geometries at the point prior to discharge, in the transition zone from vertical to hopper, as shown.

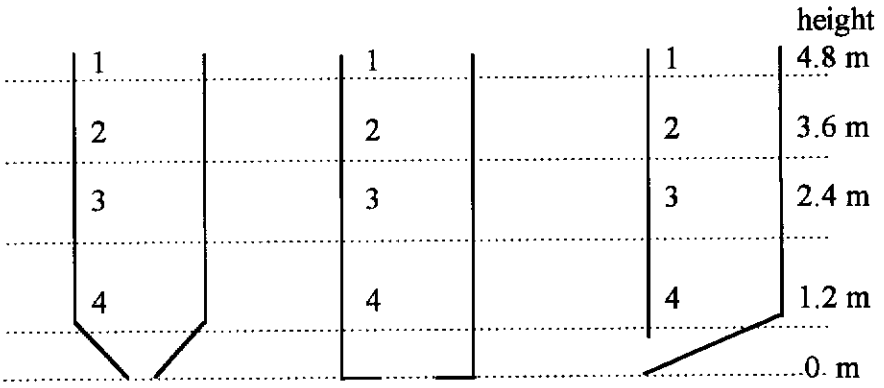

	Conical Silo	Flat Bottom Silo	Sloping Silo (Left Hand Side)
Location	Pressure (kPa)	Pressure (kPa)	Pressure (kPa)
1	20	25	36
2	32	45	54
3	45	62	60
4	135	58	46

Fig. 4.10. Silo pressure at t = 6 seconds.

4.3.4 Effect of particle size

Various particle sizes were tested to determine its effect on the flow of granules in the silo. Granular particles with three different radius (0.02 m, 0.04 m and 0.06 m) are chosen for the numerical investigation.

Figure 4.11 shows the variation of wall pressures for three sized particles. As the particle size increases, from 0.02m to 0.06m, the pressure indicated at a particular silo height is observed to increase. The increasing particle size gives an indication of higher pressure further up the silo body. This is an artefact of the size being chosen, a position between an accurate meaningful result and speed of calculation must be selected. In the current study the most optimum size was found to be 0.04m.

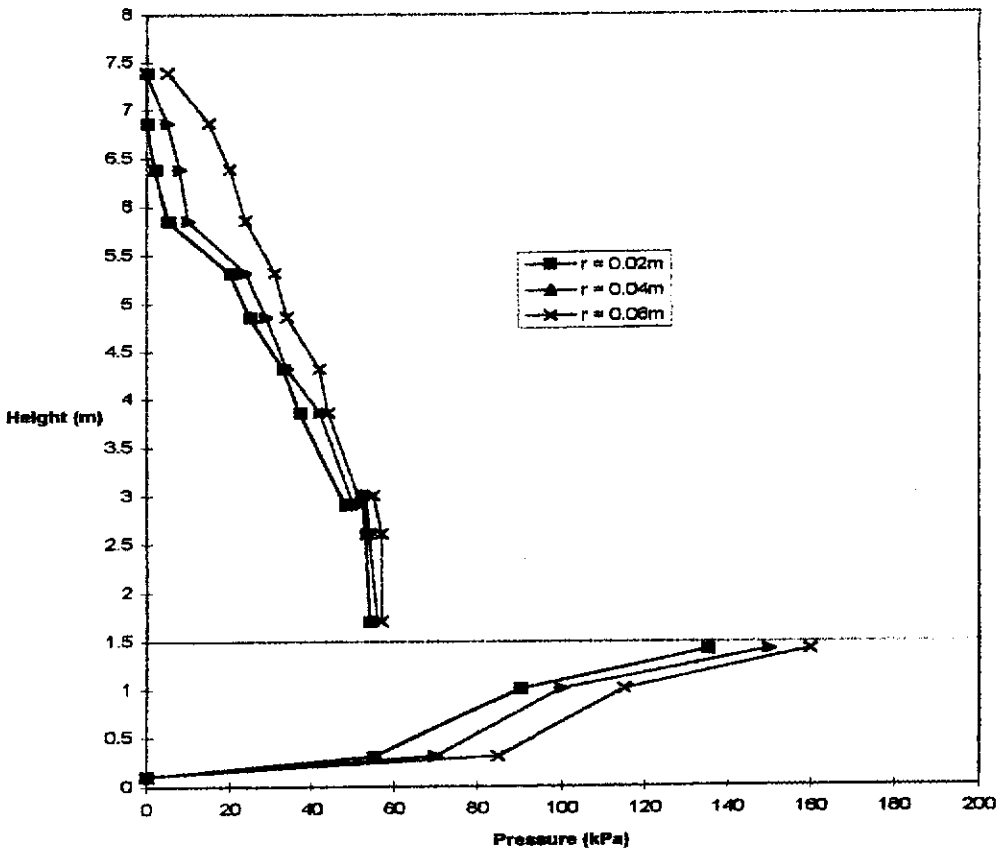

Figure 4.11. Wall pressure for varying particle size at discharge condition.

4.3.5 Summary

The discrete dynamic model developed has been used to study the flow of granular materials through silos. The flow patterns and pressure distributions obtained are in agreement with existing experimental observations. The numerical investigation results in a number of findings.

Firstly, it indicates that silo geometry is of importance and careful selection can minimise the pressure exerted on silo walls during discharging. The conical bottomed silo has the highest pressure readings in most cases. In particular, there is a large pressure increase in the transition area from the vertical silo wall to the conical discharge cone.

Secondly, the results indicate that wall friction has significant effects on wall pressures. The higher the wall friction the lower the normal wall pressure.

The results also indicate that the particle size chosen in the discrete element method is important. Use of large size particles results in quicker processing times but gives less valuable information. The processing time is faster because of the less number of particles, and hence the less number of contact calculations required. In addition, the pressure determined for the wall at a given point is less accurate, since it is based on less particles impacting with the wall. The result of one or two particles may cause a sudden change in the reading of pressure, resulting in a more irregular and less natural indication of pressure. These sudden variations in calculated pressures may be seen from the figures presented. For this study, the optimum size was found to be 0.04m, this gave reasonable computing times while providing meaningful output.

Chapter 5

CONCLUSIONS

A two-dimensional discrete dynamic model and computer program has been developed for modelling the filling and emptying processes of silos. The program has been shown to be capable of describing many features of granular flow, such as the independence of silo discharging rate on the material head. The model can be used to analyse the material flow pattern and to calculate the wall pressure and flow rate.

The model and program developed have been tested and it has been shown that the model is able to simulate granular flows in silos and produces data that is consistent with existing experimental and theoretical information. The results indicate that the silo discharge rate is independent of the material head. The flow patterns and velocity fields are in agreement with existing results. Therefore the discrete dynamic model can be used to study granular flows in silos.

A numerical investigation has been carried out to study the effect of several parameters on wall pressures and flow patterns. The investigation shows that

(1) A number of flow zones may be identified in the silos, including the plug flow zone, pipe feed zone, pipe zone and a dead zone.

(2) The area of transition from silo to hopper is marked by a change in direction of the flowing particles and a large increase in pressure.

(3) Flow begins with a movement of material down the silo, and a formation of various flow zones when the outlet is opened.

(4) Clear deadzones are observable in all silo geometries, although it is most pronounced in the flat bottom silo design only.

The results demonstrate that the difference between granular flow and fluid flow could be attributed to the existence of the internal friction in granules. In addition it has been shown that stresses on walls vary considerably over the duration of loading and discharging from a silos. These variations can be critical to the safe and efficient design of silos.

The present study indicates that the discrete element method has a number of advantages over the experimental method, namely

- Situations that are difficult or impossible to measure or determine in difficult flow scenarios may be modelled by the use of the discrete element method.
- Data from all points of a flow, at any instance of time during a flow are readily available for use in determining the characteristics of the entire assembly or of sites within an assembly.

The present study also indicates that, compared with the continuum approach, the discrete element model has the advantage that it does not require the development of a global constitutive law and that it can describe many local features of granular flow, such as the formation of voids and the velocity discontinuity planes which can hardly be described by continuum approaches. However, due to the large amount of computation required, the discrete element model at present cannot be used to model the granular flow in silos using the actual size and actual shape of granules in many practical problems. Accordingly, numerical results must be justified before using them for silo design purposes. This highly computational requirement is one of the major disadvantages of the discrete element method. Although, as computer hardware improves this is likely to become of less concern where critical and accurate predictions of flow patterns or flow characteristics are required.

There are a number of potential areas for further research including

- Development of numerical algorithms using parallel processing to increase the speed of the program.
- Development of programs which can deal with granular material of various particle shapes.

References

Ahn, H., Brennen, C.E. and Sabersky, R.H. (1991). *Measurement of Velocity, Velocity Fluctuation, Density and Stresses in Chute Flows of Granular Materials.* Journal of Applied Mechanics, Vol. 58, pp 792-803.

Ahn, H., Brennen, C.E. and Sabersky, R.H. (March 1992). *Analysis of the fully developed chute flow of granular materials.* Journal of Applied Mechanics. Vol 59.

Allen, M.P. and Tildesley, D.J. (1988). *Computer simulation of liquids.* Clarendon Press. Oxford.

Babic, M. (1990). *Discrete Element Modelling of Granular Flows.* PhD Thesis, Clarkson University.

Campbell, C.S. and Gong, A. (1986). *The stress tensor in tw0-dimensional granular shear flow.* Journal of Fluid Mechanics, Vol. 164, pp 107-125.

Campbell, C.S. and Brennen, C.E. (1985). *Chute Flows of Granular Material: Some Computer Simulations.* Journal of Applied Mechanics, Vol. 52, pp 172-179.

Campbell, C.S. (1990). *Rapid Granular Flows.* Annual Review of Fluid Mechanics. Vol. 22, pp 57-92.

Corkum, B.T. and Ting, J.M. (1986). *The Discrete Element Method in Geotechnical Engineering.* Publication 86-11, department of Civil Engineering, University of Toronto.

Cundall, P.A. and Strack, O. D. L. (1979*). A discrete numerical model for granular assemblies.* Geotechnique 29, No. 1, pp 47-65.

Dickenson, R.R. and Jofriet, J.C. (1984). *Wall Pressures in Bottom Unloading Silos.* ACI Journal, Vol. 81(1), pp 61-67.

Drucker, D.C. and Prager, W. (1952). *Soil Mechanics and Plastic Analysis in Limit Design.* Quarterly of Appl. Math., 10(2), pp 157-165.

Drake, T.G. (1994). *Granular flow : physical experiments and their implications for microstructural theories.* Journal of Fluid Mechanics, Vol 225, pp 121-152.

Haussler, U. and Eibl, J. (1984). *Numerical Investigation on Discharging Silos.* Journal of Engineering Mechanics, ASCE, Vol. 110(6), pp 957-971.

Heermann, D.W. (1986). *Computer Simulation Methods in Theoretical Physics.* Springer-Verlag. New York.

Hill, J.M. and Wu, Y.H. (1993). *Plastic Flows of Granular Materials of Shear Index n-I. Yield Functions.* Journal of Mechanical Physics. Solids. Vol. 41, No. 1, pp 77-993.

Hockney, R.W. and Eastwood, J.W. (1988). *Computer Simulation Using Particles.* Adam Hilger, Philadelphia.

Hogue, C and Newland, D. (1994). *Efficient computer simulation of moving granular particles.* Powder Technology. Vol. 78, pp 51-66.

Hopkins, M.A. (1987). *Particle Simulation.* Volume 1, Report 87-7, Department of Civil and Environmental Engineering, Clarkson University.

Hopkins, M.A. and Louge, M.Y. (1991). *Inelastic microstructure in rapid granular flows of smooth disks.* Phys. Fluids. A3(1), pp 47-57.

Hopkins, M.A. and Shen, H.H. (1986). *Constitutive Relations for a Plannar, Simple Flow of Rough Disks.* International Journal of Engineering Science. v24(11), pp 1717-1730.

Horne, R.M. and Nedderman, R.M. (1978). *Stress Distribution in Hoppers.* Powder Technology, Vol. 19, pp 243-254.

Janssen, H.A. (1895). *Tests on grain pressure in silos.* Zeitschrift des Vereines Deutscher Ingenieure, Band 39, No. 35, pp 243-254

Jenike, A.W. (1964). *Storage and Flow of Solids.* Bul. 123, Utah Engineering Expt. Sta., Univ. of Utah, November.

Jenike, A.W. and Johanson, J.R. (1969). *Bin Loads.* Journal of Struct. Div., ASCE, Vol. 94, St4, April, pp 1011-1041

Johnson, K.L. (1985). *Contact Mechanics.* Cambridge University Press. London.

Kanatani, K.I. (1981). *A Theory of Contact Force Distribution in Granular Materials.* Powder Technology. Vol. 28, pp 167-172.

Lancelot, L. and Shahrour, I. (1994). *Mechanical Behaviour of a Chemical Powder at Low Stress Levels.* Powder Handling and Technology, Vol. 6, No. 3, July-September, pp 303-308.

Langston, P.A., Tuzun, U. and Heyes, D.M. (1995). *Discrete Element Simulation of Granular Flow in 2D and 3D Hoppers: Dependence of Discharge Rate and Wall Stress on Particle Interactions.* Chemical Engineering Science. Vol. 50, No. 6, pp 967-987.

Li, T.S. (1996). *Discrete Element Modelling of Granular Chute Flow.* MSc Thesis. Curtin University of Technology.

Liffman, K., Chan, D.Y.C. and Hughes, B.D. *Force distribution in a two dimensional sandpile.* Unpublished Thesis.

Matsuoka, H. and Nakai, T. (1985). *Yield Criterion.* Soils and Foundations, 25, p 123.

Mindlin, P. and Deresiewicz, H. (1953). *Elastic spheres in contact under varying oblique forces.* Journal of Applied Mechanics (Trans ASME), Vol 79-WA APM-20, pp 327-344.

Patton, J.S., Brennen, C.E. and Sabersky, R.H. (December, 1987). *Shear Flows of Rapidly Flowing Granular Materials. Journal of Applied Mechanics.* Vol. 54, pp 801-805.

Rong, G. (1994). *Discrete Element Modelling for Flow of Particulate Materials in Bins.* PhD Thesis, University of Guelph.

Savage, S.B. (1984). *The Mechanics of Rapid Granular Flows.* Advances in Applied Mathematics. Vol 24, pp 289-367.

Schmidt, L.C. and Wu, Y.H. (1989). *Prediction on dynamic wall pressures on silos.* Int. J. bulk solids handling. Vol. 9, No. 3, pp 333-338.

Tsuji, Y., Tanaka, T. and Ishida, T. (1992). *Langrangian Numerical Simulation of Plug Flow of Cohesionless Particles in Horizontal Pipe.* Powder Technology, Vol. 71, pp 239-250.

Walker, D.M. (1966). *An approximate theory of pressure and arching in hoppers.* Chem. Engrg. Sci. Vol. 21, pp 975-997

Walker, D.M. and Blanchard, M.H. (1967). *Pressures in experimental coal hoppers.* Chem. Engrg. Sci. Vol. 22, pp 1713-1745.

Walton, O.R. and Braun, R.L. (1986). *Viscosity, granular temperature and stress calculations for shearing assemblies of inelastic frictional disks.* Journal of Rheology, Vol. 30, pp 949-980.

Zheng, X.M. and Hill, J.M. (1996). *Molecular dynamics modelling of granular chute flow: Density and velocity profiles.* Powder Technology, v86, pp 219-227.